Evolution with Time of Hydrophobicity and Microrelief of a Cation-Exchange Membrane Surface and Its Impact on Overlimiting Mass Transfer

ARTICLE *in* THE JOURNAL OF PHYSICAL CHEMISTRY B · DECEMBER 2011

Impact Factor: 3.3 · DOI: 10.1021/jp2101896 · Source: PubMed

9 AUTHORS, INCLUDING:

Natalia Dmitrievna Pismenskaya
Kuban State University
59 PUBLICATIONS **1,008** CITATIONS
SEE PROFILE

Victor Nikonenko
Kuban State University
93 PUBLICATIONS **1,757** CITATIONS
SEE PROFILE

Gerald Pourcelly
Université de Montpellier
169 PUBLICATIONS **3,080** CITATIONS
SEE PROFILE

Lasâad Dammak
UPEC-ICMPE
42 PUBLICATIONS **464** CITATIONS
SEE PROFILE

THE JOURNAL OF PHYSICAL CHEMISTRY B

ARTICLE

pubs.acs.org/JPCB

Evolution with Time of Hydrophobicity and Microrelief of a Cation-Exchange Membrane Surface and Its Impact on Overlimiting Mass Transfer

Natalia D. Pismenskaya,[†] Victor V. Nikonenko,[*,†] Nadezhda A. Melnik,[†] Kseniya A. Shevtsova,[†] Elena I. Belova,[†] Gérald Pourcelly,[‡] Didier Cot,[‡] Lasâad Dammak,[§] and Christian Larchet[§]

[†]Membrane Institute, Kuban State University, Krasnodar, Russia

[‡]European Membrane Institute, CNRS/Université Montpellier 2, Montpellier, France

[§]Institute of Chemistry and Materials, CNRS/Université Paris-Est, Thiais, France

ABSTRACT:

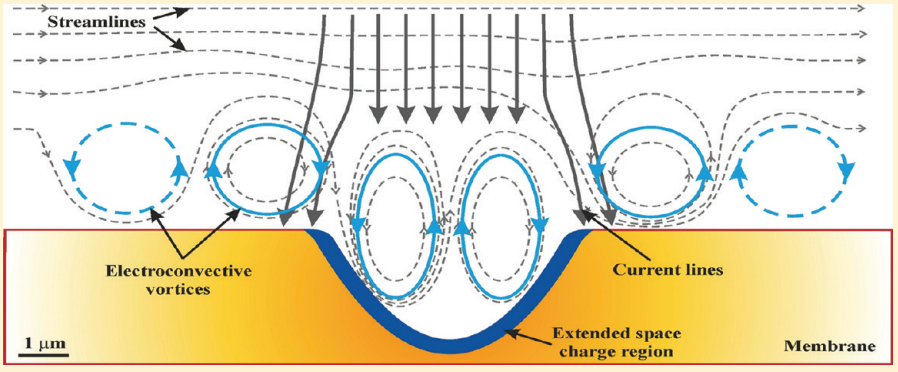

Surface properties were measured together with electrochemical characteristics of a CMX (Neosepta, Tokuyama Corp.) cation-exchange membrane. Relative hydrophobicity was controlled by the contact angle; XPS and SEM were used for characterizing chemical composition and microrelief of the surface, respectively. Voltammetry, chronopotentiometry, and mass transfer rate measurements were made as well. A "fresh" membrane and samples after 10, 25, 100, and 150 h of operation in an electrodialysis cell at an overlimiting current equal to 3 theoretical limiting currents, in a 0.02 M NaCl solution, were characterized. Some electrochemical properties were also measured for a Neosepta cation-exchange membrane, aged 2 years, in an industrial food process. It was found that the hydrophobicity of the CMX membrane has increased after the first 10 h of operation; more and more cavities of the dimension of the order of 1 μm have appeared with time testifying electrochemical erosion of the surface. The limiting current density (i_{lim}) and the overlimiting transfer rate through the CMX membrane increased with time of its operation under overlimiting current. In the case of new CMX, i_{lim} was very close to the theoretical value i_{lim}^{theor} calculated by the Lévêque equation. After 10 h of operation, i_{lim} increased by 5%, and after 25, 100, and 150 h, the increase was by 30%, 70%, and 100%, respectively. Similarly, the mass transfer rate was found to increase up to 5 times (when desalting 0.005 M NaCl under 3 V) in comparison with the theoretical value. The ensemble of data was explained by the hypothesis that the passage of intensive current produces erosion of the ion-exchange polymer forming a continuous phase in CMX. This erosion results in exposure at the surface of the other constituent of CMX: small (about 100 nm) particles of relatively hydrophobic polyvinylchloride. Increasing surface hydrophobicity facilitates the slip of electroconvective vortexes along the surface. Besides, the geometry of the cavities gives rise to appearing tangential electric force applied to the extended space charge density at cavity's walls. As the local limiting current density within a cavity is lower than at the flat surface, electroconvective vortices arise at current densities lower than i_{lim}^{theor}. With time, the number and the size of cavities increase (apparently, due to paired electroconvective vortices occurring inside them) that seems the main reason for overlimiting transfer increase.

1. INTRODUCTION

Electrodialysis (ED) is widely used in water treatment, namely in desalination of brackish river waters,[1,2] in the wine and food industry,[3,4] and in other fields.[5,6] This method is one of the main elements of "green" chemistry[7] and zero liquid discharge systems.[8] Intensification of ion transfer through ion-exchange membrane (IEM), especially when treating dilute solutions, is an important resource of improving ED technology.[9,10]

Received: October 24, 2011
Revised: December 12, 2011
Published: December 17, 2011

It is well-known that current passage through an IEM gives rise to formation of concentration profiles in the solutions separated by a membrane (the concentration polarization phenomenon). The electrolyte concentration at one membrane surface decreases and at the other one increases with increasing current density. When the concentration at the depleted surface becomes much lower than that of the bulk and even close to zero, there is a saturation of the salt diffusion flux from the solution bulk to the surface. This defines the so-called limiting current density. However, when the voltage is increasing, the current density and the mass transfer continue to rise. Intensification of ion transfer means the application of overlimiting current densities.

The mechanisms of ion transfer in overlimiting current modes are studied in a number of papers.[11−15] Four main mechanisms are considered. Two of them are linked with the water splitting:[16,17] the increase of the current density over the limiting value is provided (i) by increasing the number of charge carriers (H^+/OH^- ions) and (ii) by the exaltation effect[18] meaning an additional flux of counterions toward the membrane surface due to the effect of the water splitting products on the electric field in the electroneutral depleted solution.

Another two effects are caused by the coupling of water and electric charge transfer. Gravitational convection arises due to a horizontal gradient of the solution density;[19,20] the latter is owed to the gradient of concentration and/or to the Joule heat. Electroconvection is a result of the action of the applied electric field on the space charge occurring in the solution at the depleted membrane surface. The gravitational convection is important when the spacing between the membranes is wide and the electrolyte concentration is high, the electroconvection seems to be the main effect giving rise to overlimiting transfer in diluted solutions.[21,22] The possibility of increasing the ED transfer rate in the range of dilute solutions is especially important, as this rate is approximately proportional to the inlet concentration.[23,24] Due to experimental works of Rubinstein et al.[25] and Yossifon et al.,[26] which succeeded to visualize the electroconvective vortices near a flat membrane[25] and in nanoporous spacing formed by IEM,[26] electroconvection passed from the category of theoretical notion to that of phenomena, which can be seen by one's own eyes.

Studies carried out with laboratory-scale ED cells and semi-industrial ED apparatuses[15,27] have shown that electroconvection can produce a multifold increase in mass transfer rate in the case of diluted solutions. Actually, the electroconvection phenomenon is intensively studied and applied in nano- and microfluidic devices, such as electrokinetic micropumps,[28−30] superfast electrophoresis.[31,32] The growth of the space charge region (SCR) at the depleted ion-exchange membrane surface under the action of a direct current has made a basis for a new device of water desalination combining the approaches of electrodialysis and reverse osmosis.[33] The nonlinearity of this phenomenon allows application of alternating current for creating a one-direction electroosmotic flow.[30] This current mode is important in micropumps since enables eliminating gas emission at the electrodes.

Besides the overlimiting transfer mechanism, another important aspect considered in this paper is the evolution of the membrane properties during its exploitation under electric current.

It is well-known that usually in electrodriven processes, the membrane performance decreases with time. The loss of performance takes place under oxidizing conditions[34] or when applying a current.[35,36] Choi et al.[35] observed the growth in water splitting with long-term operation of an AMX (Tokuyama Soda) membrane in overlimiting current mode. The effect is explained by the fact that in an alkaline environment created by water splitting products (hydroxyl ions) the fixed quaternary ammonium groups of the membrane transform into tertiary and then secondary amines according to the Hoffmann mechanism.[37] This transformation was confirmed by using infrared (IR) spectroscopy. The process is intensified by the local Joule heating up to detachment of ionic groups. On the other hand, no significant changes in the structure and qualitative and quantitative composition of cation exchange membrane CMX (as well as other cation-exchange membranes with sulfonic acid groups, CM-1, CMB, HQC, sPES) during their operation under intensive current modes have been observed by using IR-spectroscopy.[37]

In this paper, we have found that the performance of a CMX membrane improved (the overlimiting ion transfer increased), at least within the first 150 h of its use in an ED cell under overlimiting currents. This unusual fact made us to carry out a rather comprehensive investigation of the evolution of membrane surface morphology and electrochemical properties of this membrane. When searching the explication of the obtained results, we have tried to make more understanding in the relation between membrane surface properties (surface morphological characteristics and contact angle) and electrochemical behavior, namely, the rate of overlimiting ion transfer.

2. THEORETICAL

2.1. Description of Concentration Polarization at the Membrane/Solution Interface. Let us consider an ED cell like that presented in Figure 1. An electrolyte solution of concentration C enters into each of the cell compartments where its average linear velocity is equal to V.

As we mentioned above, with increasing current density, the electrolyte concentration, C_s, at the membrane surface changes. When C_s becomes much lower than C, limiting current is attained. Classical theory of convective diffusion[38,39] allows one to obtain a rather simple approximate equation for calculation of the average limiting current density in a channel of length L, when the spacing between the membrane is h[39]

$$i_{\mathrm{lim}}^{\mathrm{theor}} = 1.47\frac{FDC}{h(T_1 - t_1)}\left(\frac{h^2V}{LD}\right)^{1/3} \quad (1)$$

where F is the Faraday constant, D is the diffusion coefficient, and T_1 and t_1 are the effective transport number of the counterion in the membrane and its transport number in solution. Generally, T_i is defined[40] as the current fraction carried by ion i through the interface (or the membrane in steady state) under all forces applied

$$T_i = \frac{z_iF(J_i)_s}{i} \quad (2)$$

where $(J_i)_s$ is the flux density of ion i through the interface.

T_1 is a measure of membrane permselectivity[6] toward ions of one electrical sign (counterions) in conditions where the gradients of electric potential and concentration are arbitrary. This magnitude is close to the counterion transport number in the membrane, $\bar{t}_1$. When a concentration difference ΔC occurs across the membrane, the back diffusion of salt takes place. In

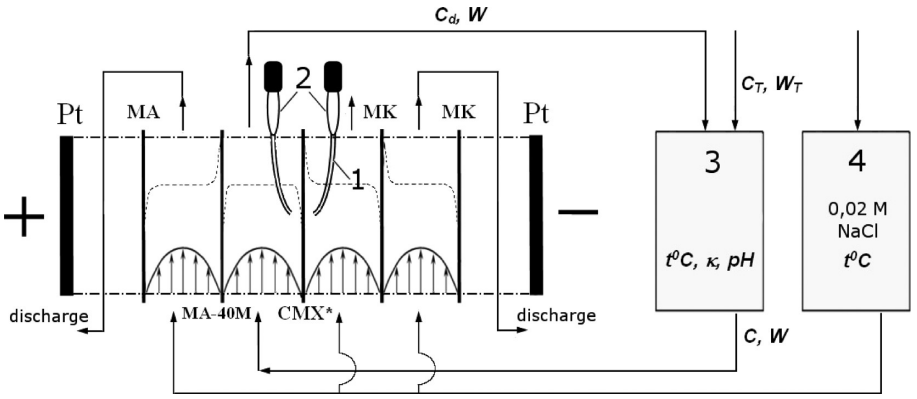

Figure 1. General scheme of the membrane cell used for measuring $I-V$, chronopotentiometric and mass transfer characteristics. The tips of Luggin's capillaries (1) are at about 1 mm from the both sides of the membrane under study (CMX*); they are connected with Ag/AgCl measurement electrodes (2). Tank (3), inserted into the desalting stream, contains a stirrer and sensors to control temperature, pH and specific electrical conductivity (κ). Tank (4) with a reserve of feeding 0.02 M NaCl solution contains a sensor to control temperature. NaCl concentration profiles are schematically shown by dashed lines; the arrows show the distribution of forced flow velocities.

this case, the relation between T_1 and $\bar{t}_1$, following from the Nernst−Planck equation in integral form, is expressed as

$$T_1 = \bar{t}_1 - P\frac{\Delta CF}{di} \tag{3}$$

where P is the diffusion permeability and d is the membrane thickness.

The actual commercial membranes are highly permselective, especially in diluted (<0.1 M) solutions, and the value of T_1 is close to unity.[6] In the case of CM2 cation-exchange membrane, whose properties are close to that of CMX, $\bar{t}_1$ in 1 M NaCl is equal to 0.996.[41]

Equation 1 is found as an approximate solution for the equation of convective diffusion in conditions of steady-state laminar fully developed fluid flow with Poiseuille quadratic velocity distribution and the no-slip condition ($V = 0$) at the solid surface, where the boundary condition $C_s = 0$ is applied.[39] No current-induced convection occurs in this case. First this problem was solved by Lévêque.[39] The origin Lévêque equation is presented as a series. However, for approximated evaluation of the limiting current density and the diffusion layer thickness in relatively short channels ($L \leq 0.01$ V h^2/D) only one term is usually sufficient. In this case the deviation between eq 1 and the numerical solution is lower than 3%,[42] whereas the experimental error in determination of i_{lim} is rarely lower than 5%.

There is another equation allowing calculation of the limiting current density, i_{lim}, known as the Peers equation[43]

$$i_{lim} = \frac{FDC^0}{\delta(T_1 - t_1)} \tag{4}$$

where C^0 is the bulk concentration and δ is the thickness of the Nernst diffusion boundary layer (DBL) in the depleting solution. In short channels considered here, C^0 is very close to the entrance concentration C.

Equation 4 is deduced from the condition of the flux continuity at the interface where the convection contribution is assumed to be zero

$$(J_i)_s = \left(-D\frac{\partial C_i}{\partial x} + \frac{it_i}{z_iF}\right)_s = \frac{iT_i}{z_iF} \tag{5}$$

x is the normal to the surface coordinate.

The middle part of eq 5 refers to the solution, the right-hand part to the membrane. The concentration gradient of the counterion (1) at the membrane surface may be written as

$$\left(\frac{\partial C_1}{\partial x}\right)_s = -\frac{C_1^0 - C_{1s}}{\delta} \tag{6}$$

According to eq 6, δ is the distance from the membrane to the intersection point of the tangent drawn to the concentration profile at the interface with the line corresponding to the bulk solution concentration. Substituting eq 6 into eq 5 and setting $C_{1s} = 0$ leads to eq 4.

Equation 4 is valid for the local as well as the average limiting current density. For the local value of δ, the following equation results from the Lévêque solution

$$\delta_{Lev} = 1.02\left(\frac{LDh}{V}\right)^{1/3} \tag{7}$$

According to eq 7, δ_{Lev} is zero at the channel entrance and increases with increasing L.

The substitution of the local value of δ, eq 7, into eq 4 and the integration of the latter along the distance from the channel entrance results in obtaining the average on length L limiting current density, eq 1. Thus, eqs 1−7 are self-consistent. If i_{lim}^{theor} expressed by eq 1 is set into eq 4, the corresponding value of δ in this equation takes the meaning of an effective average value of the DBL thickness in a desalination channel of length L.

Actually, eq 4 is held not only at the limiting current density, but also at the overlimiting current densities. It is known that the coupling between the volume and ion transfer (gravitational and/or electroconvection) enhances the delivery of fresh solution to the membrane surface, increasing the current density.[44,15] The deduction of eq 4 does not explicitly take into account the contribution of convection. However, this contribution may be accounted implicitly by assuming that δ decreases with increasing current-induced convection. With decreasing δ, under the action of coupled convection, the limiting current density rises, and in this way we can explain the enhancement of mass transfer rate in overlimiting current regime.

The application of the Rubinstein model,[45] in which the deviation from the local electroneutrality is taken into account by the Poisson equation, to description of experimental $I-V$

curve has shown[14] that after reaching the plateau of the curve, the value of i becomes very close to i_{lim}. Hence, assuming $i \approx i_{lim}$, it is possible to evaluate the effective value of δ from eq 4.[14]

The emergence of H^+ and OH^- ions near the interface disturbs the electric field that can increase (exalt) the salt counterion transfer: e.g. the OH^- ions generated into the depleted diffusion layer at a cation-exchange membrane attract the salt cations from the solution bulk toward the interface.[18] When taking this effect into account, the limiting and overlimiting current density of salt counterions ($i_{1,lim}$) can be described by the following equation[12,14] deduced under assumption of zero co-ion transport through the membrane

$$i_{1,\mathrm{lim}} = \frac{2FD_1C^0}{\delta} + \frac{D_1}{D_w} i_w \tag{8}$$

where D_1 is the diffusion coefficient of the salt counterion and D_w and i_w are the diffusion coefficient and the partial current density of the product of water splitting generated into the depleted diffusion layer, the OH^- ion in the case of cation−exchange membrane.

Equations 4 and 8 can be deduced within the Rubinsten[45] model, when considering only the electroneutral part of the DBL.[14] Hence, an important remark should be done to the sense of the effective thickness of DBL in these equations: it is the thickness of the electroneutral part of the overall diffusion layer. Under high voltages, the extended SCR (forming the charged part of the DBL) can be comparable with its overall thickness: under 8 V over a pair cell with h = 0.5 mm and 0.002 M NaCl, these values were found to be 2 and 14 μm, respectively.[14]

2.2. Gravitational Convection. Consider a solution layer situated between two smooth solid plates where a density gradient occurs for some reason. In fluid mechanics, it is known[19] that when the plates are vertical and the density gradient in the solution is horizontal, the gravitational convection arises without threshold, no matter how small is the density gradient. When the plates are horizontal and the density gradient is vertical, two cases are possible. If the lighter solution sublayer (normally, the depleted DBL) is on the top of the solution layer (hence, just under the top plate), no convection arises. If the lighter sublayer is at the bottom, there is a threshold in development of the gravitational convection determined by the Rayleigh number

$$Ra = GrSc = \frac{\Delta\rho}{\rho}\frac{gX_0^3}{\nu D} \tag{9}$$

where Gr and Sc are the Grashof and the Schmidt numbers, respectively; g is the free-fall acceleration, ν is the kinematic viscosity, D is the electrolyte diffusion coefficient, X_0 is the characteristic distance where the variation in the solution density (ρ) takes place, $\Delta\rho$ is the variation of ρ within X_0. If the region of solution density variation spreads from the one plate to the other, X_0 is equal to the distance between the plates, h. In the case of desalination/concentration channel between two membranes (such as shown in Figure 1), X_0 may be associated with the DBL thickness.[46,47]

The system (with horizontal plates and the density increasing from the bottom to the top of the solution layer) is stable if $Ra < Ra_{cr} = 1708$: the characteristic time, which is necessary for diffusion relaxation of a density fluctuation in a small solution volume, is less than the characteristic time of floating-up of this volume.[19] Hence, a density fluctuation once appearing dissipates, and no gravitational convection occurs in this case. If $Ra > Ra_{cr}$, the volume with negative fluctuation in density lifts with acceleration. In this case, the density within the lifting volume increases more slowly than the density in the environmental solution. Hence, the amplitude of a small perturbation increases with time, and periodic cellular vortex structure (the Bénard convection cells) arises in the solution.

2.3. Mechanism of Electroconvection. Electroconvection occurs as electroosmosis of the first or second kind.[48,49,44] Electroosmosis of the first kind is due to the action of an external electric field on the space charge located in equilibrium electric double layer (EDL). In the case of second kind, known also as induced-charge electroosmosis,[50,51] the external electric field acts on the space charge in an extended nonequilibrium space charge region, the growth of which over the limits of the equilibrium EDL is caused by the same external field.

The paper[11] by Rubinstein and Zaltzman is one of the most important in the field as the authors have anticipated a scenario of the development of electroconvection with time and with increasing voltage, which was approved later experimentally by Belova et al.[12] They deduced theoretically the existence of three different regimes of electroconvection. Regime 1 is attained, in the case of homogeneous membranes, just after overcoming a certain threshold value of the voltage, which corresponds to the transition from stability to instability. In this regime, a small perturbation of velocity causes development of paired vortices near the membrane surface, which after oscillatory readjustment in the size and shape become steady-state. This process manifests itself in decaying oscillations of the electric current through the interface: after several oscillations the current density (or the potential difference, if the current is maintained constant) reaches a constant stationary value. Regime 2 occurring at somewhat higher voltages is characterized by nondecaying regular oscillations and regime 3, at still higher voltages, by chaotic oscillations of higher amplitude. The size of vortices increases with increasing current density/voltage, hence, they more and more effectively produce mixing of solution near the membrane surface. This results in delivering fresh solution to the surface and reducing the effective thickness of diffusion boundary layer, δ. While the increase in current density normalized to the limiting current density considered in the theory of Rubinstein and Zaltzman is rather small,[11] the absolute value of overlimiting current increase may be quite significant, since the limiting current density, inversely proportional to δ, increases with increasing voltage.

Recent studies have shown that the intensity of electroconvection depends strongly on the membrane surface properties. The first parameter is the surface heterogeneity. Electrical heterogeneity can be produced by alternation of well and poorly conducting regions on a flat surface. In this case the theory[52,14] predicts hastening the onset of overlimiting transfer because of the inherent inhomogeneous distribution of the space charge density on the membrane surface. This follows from the general necessary condition of the electroconvection occurrence: for the appearance of electroconvection, it is necessary that the curl of the product of the electric field and the space charge density should be nonzero.[14] Note that in the case of flat homogeneous surface, a nonzero curl arises due to instability of quiescent electric conduction.[11] Another possibility of an early onset of overlimiting transfer relates to relief/profiled/undulated membrane surface.[48,11,13] In this case, a tangential electric field component occurs, and its application to the SCR near a sloping

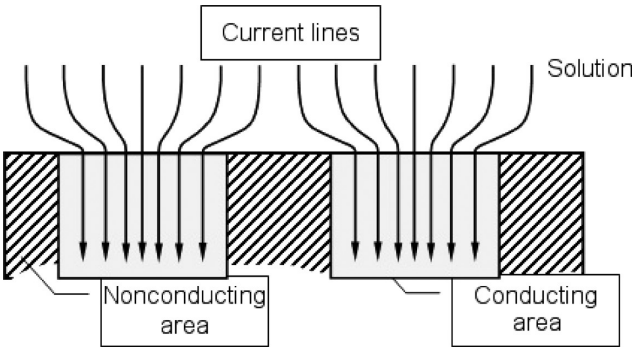

Figure 2. Scheme of the current line distribution close to a heterogeneous membrane surface. Reprinted with permission from ref 58. Copyright 2005 Elsevier.

surface brings liquid in motion much more effectively than it takes place at a flat surface.[44] The size of these inhomogeneities following numerical calculations based on the Nernst−Planck and Navier−Stokes equations[14,11,53] should be of the same order than the diffusion layer thickness. The theory of Rubinstein and Zaltzman[11] predicts the earlier onset of overlimiting conductance and a shortening of the plateau length in the $I-V$ curve (which may be considered as the measure of ability of the system to pass from mainly diffusion to mainly electroconvective mechanism of mass transfer) if the surface is undulated. Following their calculations, the effect is maximum when the period of undulation is proportional to the DBL thickness.

Actually, the rate of mass transfer in an ED cell with a profiled membrane having surface with conic "hills" of about 0.5 mm of height[54] is 6−10 times higher than that in a cell with flat membranes separated by a nonconducting net spacer.[55] Similar results were obtained by Strathmann and Grabowski.[56,23]

Balster et al.[13] have found that the creation of undulations on the surface of a homogeneous membrane leads to reduction of the $I-V$ plateau length up to 60% compared to that of a flat membrane. They attributed the effect to the enhancement of overlimiting mass transfer due to electroconvection. The dimensions of the relief elements assuring the decrease of plateau length were in the range of 50 to 200% of the DBL thickness, in good accordance with the theory.[11,53,14]

At the same time, the electric heterogeneity increases locally concentration polarization (effect of funnel, Figure 2[57,58]). In the case where the surface fraction of conducting area is f_c and the other part of the surface is nonconducting (in the case of Russian heterogeneous membrane MK-40 f_c is in the range 0.2−0.3),[58] the local current density through conducting area is $i_{loc} = i_{av}/f_c$, where i_{av} is the average current density over all the surface. Tangential diffusion of the salt to the conducting regions and more intensive electroconvection near electrically inhomogeneous surface enhance the mass transfer and increase the local limiting current through conducting regions. However, if the fraction of nonconducting surface is high, the average limiting current density may be lower than that in the case of homogeneous flat membrane.

The second property affecting electroconvection is the surface hydrophobicity. Recently, we have shown[15] that the overlimiting transfer rate strongly depends on the degree of membrane surface hydrophobicity: the more the surface hydrophobicity (characterized by the contact angle), the more the limiting and overlimiting current density under the same potential difference. These results are explained by the fact that slip of fluid at hydrophobic surface facilitates the current-induced convection. The slip of fluid at the surface is a general phenomenon. To describe it, Navier has introduced the slip boundary condition in the form[59]

$$u_{slip} = b(\partial V_y/\partial n)_s \quad (10)$$

which relates the fluid tangential velocity u_{slip} at the surface and the shear strain rate normal to the surface, $\partial V_y/\partial n$, via the slip length b; the velocity of the surface is set to zero. $b = 0$ relates to the no-slip condition, and u_{slip} increases with increasing b.

It is known that in macroscopic systems the Navier slip is negligible.[39] However, it becomes important in micro- and nanometer channels.[60,59]

The slip velocity depends strongly on the degree of surface hydrophobicity. On the hydrophobic surface, there is a repulsion of water molecules from the surface that reduces or eliminates the slow-down effect of the surface.[61,62] The values of slip length reported vary from several nanometers[62] to as high as several tens of micrometers.[63,64]

Analysis of the literature[65,66] suggests two main factors affecting the hydrophilic/hydrophobic balance. The first one is the chemical nature of the surface: polar groups of polymers are hydrophilic, whereas nonpolar groups are hydrophobic. The second no less important component is micro- and nanorelief of the interface. According to Wenzel,[67,65] roughness can enhance the hydrophobicity, if the water contact angle on the smooth surface of the given material is greater than 90°.[59,68] And, conversely, if the corresponding angle is less than 90°, roughness increases the hydrophilicity.

Another parameter important in development of electroconvection is the stokesian radius of hydrated counterion. The greater this radius, the larger number of water molecules are involved in motion with one counterion, and the more intensive is electroconvection. Choi, Lee, and Moon[69] have found that in the case of a homogeneous CMX membrane, the $I-V$ plateau length (characterizing the ability of the system to pass from mainly diffusion to clearly convective transfer) decreases in the range HCl > KCl > LiCl > $CaCl_2$ > $MgCl_2$ > $AlCl_3$. Hence, the H^+ ions, having a small stokesian radius, only hardly can cause electroconvection, while the Al^{3+} ions are able to give a prompt rise to electroconvection.

3. EXPERIMENTAL SECTION

3.1. Membranes. The object of the study is a homogeneous CMX membrane (Neosepta, Astom, Japan).[70] According to Lue et al.,[71] the membrane contains 45−65% of sulfonated styrene-divinylbenzene randomly cross-linked copolymer and 45−55% of polyvinylchloride (PVC). It is manufactured by the paste method.[72] The paste contains a monomer with functional groups, divinylbenzene as a cross-linking agent, a radical polymerization initiator and finely powdered polyvinylchloride. The paste is coated onto a PVC reinforcing network, and the monomers are copolymerized and then sulfonated.[72] The network with the mesh step 200 μm and the threads of diameter of about 30 μm are clearly seen in the cross section of the membrane (Figure 3).

Ion exchange capacity of the wet CMX membrane is equal to 1.62 ± 0.1 meq g_{dry}^{-1} (in H^+ form)[73] and its thickness is 176 ± 5 μm. The fixed sulfonic acid groups of the membrane are characterized by low catalytic activity in relation to the H^+ and OH^- ions generation in "water splitting".[16,74]

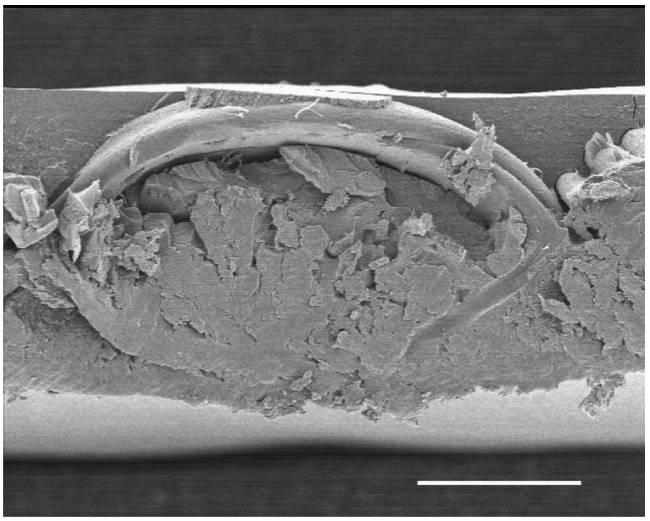

Figure 3. SEM image of cross section of the CMX membrane surface; the threads of reinforcing cloth are seen. Scale bar = 85.7 μm.

3.2. Visualization of the Surface; Chemical Composition of the Membrane Surface and the Bulk. Visualization of surface and cross section of the membrane is carried out by 2D scanning electron microscopy (SEM); a LEO (ex LEICA, ex CAMBRIDGE) type S260 microscope was used. The samples were previously dried in vacuum and coated with an ultrathin layer of platinum in order to impart electronic conduction to the surface. This allows decreasing the electron beam energy required during imaging, to prevent the accumulation of electrostatic charge on the specimen surface. Thus the deposition of the Pt layer results in improving contrast of imaging and in avoiding the distraction of the membrane polymer under the action of the electron beam.

The chemical composition of an air-dried CMX membrane was studied by FTIR spectroscopy (FTIR); the instrument used was TENSOR27 (Bruker).

The chemical composition of the membrane surface layer was studied by X-ray fluorescence (XFS) and X-ray photoelectron spectroscopy (XPS). In the first case, we used scanning electron microscope Hitachi S-4500 I FE-SEM with an attachment QUANTAX 200. XPS was performed using an AXIS Ultra DLD electronic spectrometer.

3.3. Contact Angles. The contact angles (CA) on the surface of the CMX membrane, in the sodium form, were measured by the sessile drop method. A water drop of approximately 7 μL in volume was applied from a height of 0.7 cm on the membrane surface (Figure 4). This technique[75] differs from the traditional ones[76,77] in that the membrane is in a swollen state, preequilibrated with a solution (0.02 M NaCl). The membrane is removed from the solution just before the measurements. It is placed in a closed optically transparent box on a filter paper, which is in contact with the same 0.02 M solution of NaCl. The residual solution film on the membrane side faced to the liquid dozer is quickly removed by air-blast.

The images obtained with a digital video camera are processed using computer program ImageJ to improve the contrast of the contours of the drop. After 30 s past application of a drop, the photo of the drop profile was taken, and then the contact angle of water on the investigated membrane was measured. The experiment was repeated no less than 10 times. The drop was placed

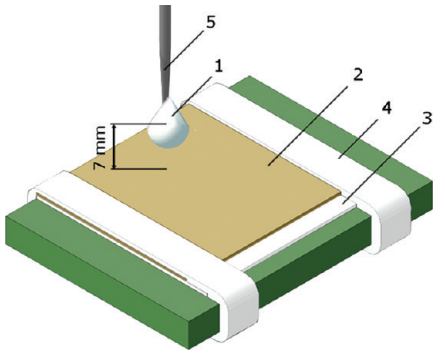

Figure 4. Set-up for applying a water drop (1) on the surface of a membrane (2). The membrane lies on a sheet of filter paper (3) fastened by two bands of filter paper (4). All pieces of filter paper are impregnated with a solution, in which the membrane was equilibrated earlier. The capillary (5) for dosing water is situated at about 7 mm above the membrane surface.

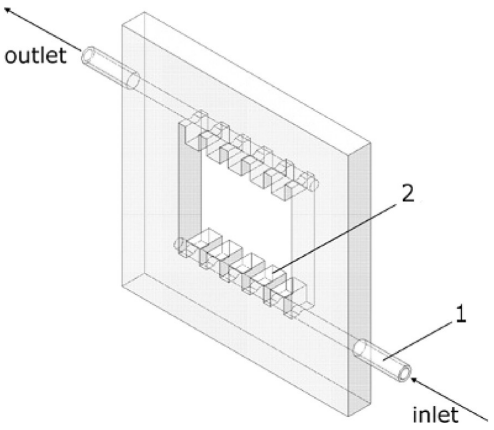

Figure 5. Plastic frame with connecting pipes (1) and comb-shape stream spreaders (2).

onto various parts of the membrane surface; then the average value of contact angle and the standard deviation was calculated.

This method allows us to keep the membrane in conditions close to thermodynamic equilibrium with a solution. These conditions are similar to the real state of membranes in electrodialysis cell, where they are always in contact with water. If a drop is applied on dry membrane surface, the water contained in the drop may change locally the state of the surface: the contact angle values may be distorted by the reorientation of polymer chains in the near surface layer.[76] The effects of surface skin reorganization in contact with water are investigated mainly for Nafion materials,[76,78,79,77] and our experiments shows that other ion exchange membranes demonstrate a similar behavior.

3.4. Current−Voltage and Chronopotentiometric Curves. Current−Voltage Curves (CVC) and Chronopotentiometric (ChP) curves were measured in a direct-flow six-compartment cell without spacer between the membranes (Figure 1) described earlier.[12,58,80]

The compartments are formed by five membranes each of them is inserted between two plastic frames (Figure 5) with connecting pipes and comb-shaped input-output devices. The thickness of the frame is 5.0 mm, which together with the thickness of two sealing gaskets makes the spacing between two neighboring membranes, h = 6.3 mm. The square aperture

(S) of the frame available for electric current flowing is 2 × 2 cm × cm. The average flow velocity (V) between two neighboring membranes used in all experiments was 0.36 cm s^{-1}, so that the Reynolds number $Re = 2hV/\nu$ (ν is the water kinematic viscosity) was equal to 45.

The CMX membrane under study forms a desalination channel (DC) together with an anion-exchange MA-40M membrane characterized by a low water splitting in overlimiting current regimes.[12,76] Auxiliary anion-exchange (A) and cation-exchange (C) membranes prevent the penetration of electrode reaction products from platinum plane anode and cathode to the central DC. The concentration profiles formed under a direct current are schematically shown in Figure 1. The tips of the Luggin's capillaries (1) with an external diameter of 0.8 mm are located in the next to the CMX membrane compartments near the center of the membrane at a distance of about 1 mm from its surface. The Luggin capillaries are connected with Ag/AgCl electrodes (2) used to measure the potential difference (pd) across the CMX membrane and two adjacent solution layers.

In the actual study, the membranes were positioned horizontally, the anode at the bottom and the cathode at the top of the cell, so that the adjoining depleted diffusion layer was under the studied CMX membrane to avoid gravitational convection in the depleted solution in the vicinity of the membrane. Of course, the lighter depleted layer adjacent to the top of the MA-40M membrane (Figure 1) can go up and create convection. However, the Rayleigh number for the applied conditions (C_{NaCl} = 0.02 mol dm^{-3}, $X_0 = \delta \approx 250$ μm, $D = 1.6 \times 10^{-5}$ cm^2 s^{-1}) is approximately equal, according to eq 9, to 340. When evaluating $\Delta\rho \approx 3.6 \times 10^{-3}$ g cm^{-3}, we have taken into account that the difference in the density between a 0.02 M NaCl solution (in the solution bulk) and water (at the depleted MA-40 M surface) is about 0.95×10^{-3} g cm^{-3}, under the same temperature; and that this difference can be higher due to Joule heating of the depleted solution at the membrane. If the increase in temperature at the interface is assumed to be 10 K in comparison with the solution bulk, the decrease in the density is about 2.6×10^{-3} g cm^{-3}. The obtained value of Ra = 340 is significantly lower than Ra_{cr}=1708, hence, we can expect that no gravitational convection occurs in the system. Note that similar estimation of the Rayleigh number were made by Rubinstein et al.[46]

The comb-shaped inlet−outlet devices (Figure 5) provide laminar steady-state fluid flow in the cell compartments. To avoid the pulsations of velocity by pumps, the solution passes through the cell by gravity, flowing from an intermediate tank situated sufficiently high over the cell. It was shown[12] that in these conditions and when the membranes in the same cell as presented in Figure 1 was positioned horizontally so that the adjoining depleted lighter diffusion layer under the studied membrane (Neosepta homogeneous anion-exchange AMX membrane, produced by Tokuyama Corp., Japan), the experimental limiting current density, i_{lim}^{exp}, and that calculated according to the Lévêque equation, eq 1, were very close (the deviation was not higher than 7%) for 0.005 M as well as for 0.1 M NaCl solutions. The value i_{lim}^{exp} was found by the intersection of the tangents drawn to the initial part of the $I-V$ curve and its "plateau". Similar results were obtained in the case of AMX/0.02 M NaCl system.[47] However, when the membrane was in the vertical position, in the case of 0.1 M NaCl the experimental limiting current density was about 30% higher than that theoretical.[12] This deviation was attributed to gravitational convection significant in relatively concentrated solutions.

$I-V$ curves and chronopotentiograms were measured in the range of current densities from 0.25 to 4 i_{lim}^{theor}.

When comparing the electrochemical behavior of different membrane systems, it is convenient to use, instead of the total potential drop $\Delta\varphi_{tot}$, a reduced value $\Delta\varphi'$. In the case of voltammetry (CVC)

$$\Delta\varphi' = \Delta\varphi_{tot} - iR_{ef} \quad (11)$$

where i is the electric current density and R_{ef} is the differential resistance of the membrane system found by the slope of the initial part of the $I-V$ curve, at $i \rightarrow 0$. It includes the ohmic resistance of the space (membrane + solution) between the Luggin's capillaries, and the "diffusion" resistance of the interphase boundaries and the depleted and the enriched diffusion layers.[12]

In the case of chronopotentiometry

$$\Delta\varphi' = \Delta\varphi_{tot} - \Delta\varphi_{ohm} \quad (12)$$

where $\Delta\varphi_{ohm}$ is the ohmic resistance of the nonpolarized membrane system, which is found by the extrapolation in coordinates $\Delta\varphi_{tot} - \sqrt{t}$ to zero time (the time t is counted off from the moment of the current switch-on).[81]

In this study, we have chosen the use of rather diluted solutions, the NaCl concentration was equal or lower than 0.03 mol dm^{-3}. This choice was made since we expected that the main effect enhancing mass transfer at overlimiting current densities was electroconvection. The intensity of electroconvection, as it was mentioned in section 2.3, increases with decreasing concentration (due to increasing thickness of the SCR), whereas the contribution of gravitational convection becomes negligible, especially if some special conditions are met. On the other hand, the practical importance of the increase in the mass transfer rate in such applications as electrodialysis, diffusion dialysis, reverse electrodialysis for power conversion and other grows with diluting feed solution.[73] The reason is that in electromembrane systems operated in the low concentration range (<0.5 M), the mass transfer rate is, in the first approximation, proportional the feed concentration, eqs 1 and 4.

When measuring $I-V$ and ChP curves, we applied a 0.02 M NaCl solution. For intermembrane spacing h = 6.3 mm and V = 0.36 cm s^{-1}, the values of i_{lim}^{theor} and the average thickness of DBL, δ, calculated by eqs 1 and 4 are equal to 2.0 mA/cm^2 and 260 μm, respectively. For these calculations, the following parameters were used: $D_{NaCl} = 1.61 \times 10^{-5}$ cm^2 s^{-1} (related to the infinitely dilute solution), $T_{Na}^{C} = T_{Cl}^{A} = 0.99$ (see eq 3 and section 4.3), t_{Na} = 0.396, t_{Cl} = 0.604,[82] where the superscript A refers to the anion-exchange membrane and C to the cation-exchange one. It is taken into account that the counterion transport numbers in ion-exchange membranes in diluted solutions are very close to unity.[41]

3.5. Concentration Dependence of the Mass Transfer Coefficient. The concentration dependence of the mass transfer coefficient is obtained in the same cell as that used for $I-V$ and ChP measurements. The difference in the realization of the procedure is in the use of an intermediate tank (3), Figure 1, through which the desalinating stream was circulating. The intermediate tank was completed with a stirrer and sensors to control temperature, pH and electrical conductivity of the solution. Before the experiment, the tank, the central DC compartment of the cell and the hoses were filled with 100 mL of 0.03 M NaCl solution. Then a constant voltage controlled by the pd measured with the Luggin's capillaries (Figure 1) was

applied and electrodialysis process was realized at 25 ± 0.5 °C maintained in the tank. The solution circulated through the tank and the Desalination Compartment (DC) of the cell with flow rate W. The salt concentration in the tank decreased with time because of the electrodialysis desalination: the outlet concentration, C_d, was lower than the inlet one, C. Besides, there were changes in pH of the solution passed through the DC due to different rates of water splitting at the cation-exchange (CMX) and the anion-exchange (MA-40M) membranes. In order to maintain pH = 7 in the solution in tank (3), alkaline (NaOH) or acid (HCl) solution were added into the tank, depending on the sign of the pH changes in the outlet solution. The desalination process was realized in quasi-steady-state conditions, the amount of the solution put in the system was so that allowed us to keep a slow (less than 1%/min)[80,83] decrease in the electrolyte concentration of the solution in the desalting stream. Total duration of every run was about 8−10 h. The electric current, as well as the specific conductivity of the solution (converted then into the NaCl concentration) in the tank were measured as functions of time.

The mass transfer rate may be found from the rate of the concentration decrease in the tank. Really, the salt concentration in the tank varies due to ion transfer through IEMs in the cell and due to addition of alkaline (or acid) solution into the tank in order to maintain pH 7. The description of material balance in the tank conducts to the equation

$$k_1 = \frac{i_1}{FC} = -\frac{V_{sol}}{SC}\frac{dC}{dt} + \frac{c_T W_T}{SC} \quad (13)$$

where i_1 is the partial current density of counterion (1) through the membrane under study; C, the current salt (NaCl) concentration in the tank; k_1 (defined as i_1/FC), the mass transfer coefficient, characterizing the salt counterion transfer rate through the membrane under study; V_{sol}, the volume of solution in the desalting stream (including its volume in the tank, in the desalting compartment of the cell and in the hoses); W_T and c_T are the volume rate and the concentration of the solution (NaOH or HCl) added into the tank to maintain pH 7; S, the membrane active surface. The first term in eq 13 showing the rate of concentration variation in the tank depends on the rate of ED desalination (the term in the left-hand side of the equation) and the rate of alkaline or acid addition.

Equation 13 assumes that there is no salt co-ion flux through both membranes forming the desalination compartment. This equation is applied if the mass transfer coefficient is calculated for the salt counterion passing through the membrane, which generates less H^+ and OH^- ions than the other one forming the desalination compartment. It is the case of Na^+ transfer through the CMX membrane making a pair with a MA-40M membrane. In this case, NaOH is added in the tank to compensate the excess of H^+ ions produced at the MA-40M membrane. To calculate the mass transfer coefficient of Cl^- ion for the MA-40M only the first term in eq 13 should be taken into account, as no Cl^- is added in the tank, and eq 13 becomes

$$k_1 = \frac{i_1}{FC} = -\frac{V_{sol}}{SC}\frac{dC}{dt} \quad (14)$$

3.6. Diffusion Permeability. The diffusion permeability of the CMX membrane before and after its operation in intensive current modes was measured in a cell[84] with the same type of frames as shown in Figure 5. The only difference was in the fact that the aperture was 2.7 × 2.7 cm instead of 2.0 × 2.0 cm, and the cell contained two compartments instead of six ones in the case of electrochemical measurements. A 0.5 M NaCl solution circulated (through an intermediate tank) from one side of the membrane under study, and (initially) pure water circulated (through another intermediate tank) from its other side. The volume of the 0.5 M NaCl solution was sufficiently high to make negligible the variation of the concentration in this stream with time. The salt flux through the membrane was controlled by the rate of the increase of its specific electric conductivity in the salt-receiving stream.

In the case of the treated under current membrane, the side, which previously faced the desalination channel, was in contact with pure water, whereas the side, which faced the concentration channel, was in contact with the 0.5 M NaCl solution.

3.7. Overall Procedure of Measurements. The CMX membrane was operated during some time (10, 25, 100, and 150 h) in a 0.02 M NaCl solution under an overlimiting current density i, which is 3 times higher than i_{lim}^{theor}. The schedule of the experiments is represented in Table 1.

4. RESULTS AND DISCUSSION

4.1. Evolution of the Relief and the Hydrophilic/Hydrophobic Balance of the CMX Membrane Surface. Figures 6 and 7 show SEM photographs of the surface (Figure 6) and the cross sections (Figure 7) of membranes, in particular, their near-surface layer (Figure 7a,b). Figure 8 shows the roughness of the surface relief of an untreated and a treated under current membranes. The microphotographs were processed with GIMP 2 program in order to increase the contrast and then calculate the number of white and dark pixels. In this way the fraction of the surface occupied by the cavities was determined (Table 2).

These data show that the exploitation of the CMX membrane under intensive currents results in changes of surface topography at the micrometer scale. Indeed, the surface of the untreated membrane (which underwent only a standard salt pretreatment according to paper,[85] but was not exposed to the electric current) in the micrometer scale is rather homogeneous (Figure 6a). Only very small number of cavities may be observed (Table 2). The surface of the current-treated membrane (Figure 6b,c) demonstrates the cavities, the number and the size of which increases with time (Figures 6b,c and 7). The diameter and the depth of the cavities can attain 2 μm (Figure 7c).

The grains visualized on the cross sections of the fresh and the current-treated membranes can be attributed to the PVC used as a filler of the membrane.[72,86] The material binding the grains of PVC seems to be an ion exchange polymer, which is a functionalized styrene- divinylbenzene copolymer according to Mizutani.[87] The reason for the evolution of the surface shown in Figure 6b,c is, apparently, the electrochemical degradation of the copolymer, constituting the matrix of the ion-exchange material. The rupture of ion-exchange polymer chains at the membrane/solution boundary may be provoked by the presence of a high electric field and H^+ (OH^-) ions generated at this interface in overlimiting conditions. This process is similar to that observed in fuel cells for polymers, which are chemically stable under normal conditions.[88]

It seems that there is no degradation of PVC during the operation of CMX under current. This is evidenced by the fact that the

Table 1. Schedule of the Experiments with "Fresh" and Treated under Overlimiting Current CMX Membranes

	duration of the CMX membrane treatment under overlimiting current, hrs				
technique[a]	0	10	25	100	150
SEM	+			+	+
XPS	+			+	
FTIR	+			+	
CA	+		+	+	+
diffusion permeability	+			+	
CVC	+	+	+	+	+
ChP	+	+	+	+	+
mass transfer measurements		+		+	

[a] SEM: scanning electron microscopy, XPS: X-ray photoelectron spectroscopy, FTIR: Fourier infrared spectroscopy, CA: contact angles, CVC: voltammetry (current−voltage curves), ChP: chronopotentiometry.

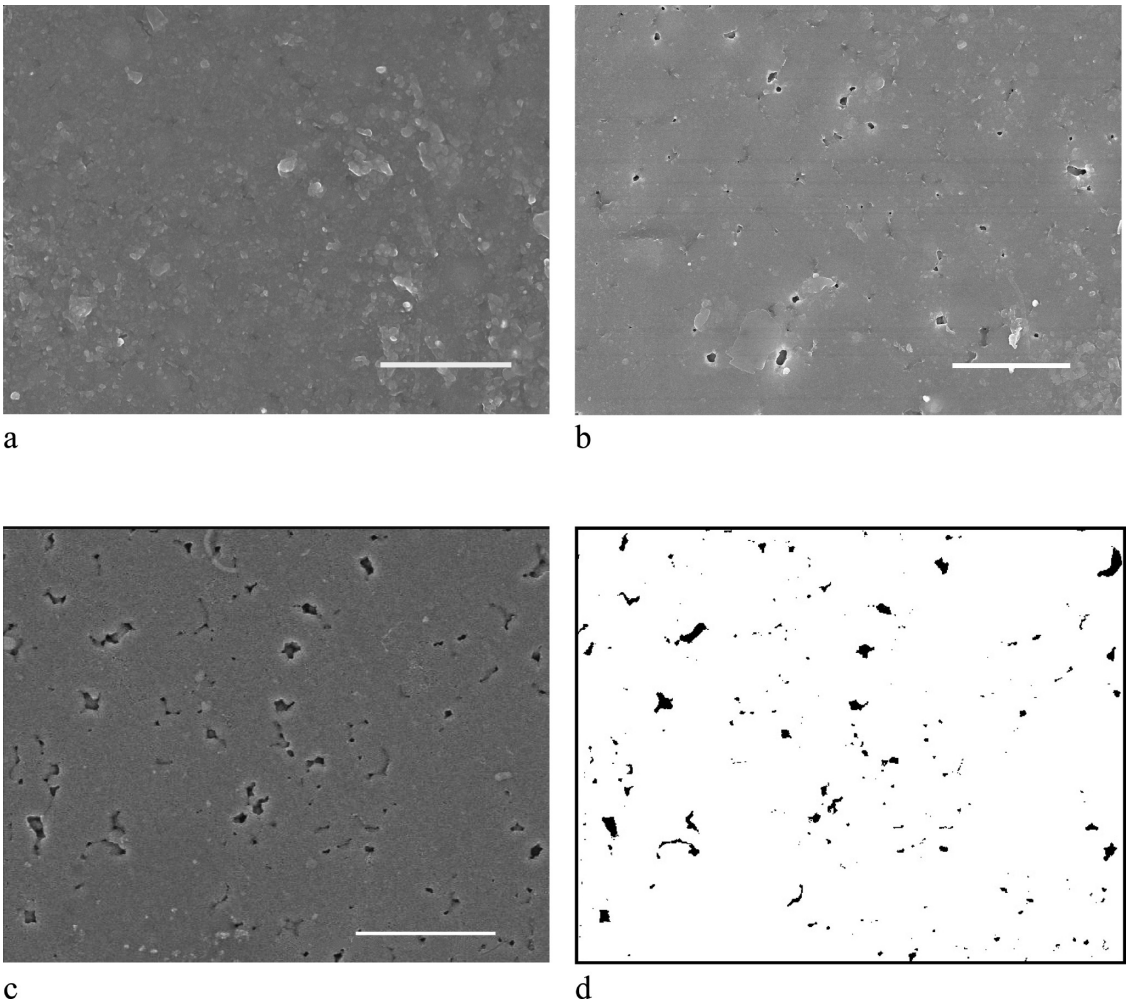

Figure 6. SEM images of the surface of the CMX membrane before (a) and after (b and c) its operation under overlimiting current during 100 h (b) and 150 h (c). (d) is an image of microphotography (c) obtained by its processing with GIMP 2 program. Scale bar = 6 μm.

current-treated CMX membrane does not darken, in contrast to the AMX membrane (manufactured from the same styrene-divinylbenzene polymer and filler PVC as the CMX[72]), which becomes dark under current.[86] The darkening of AMX is explained by the action of OH^- ions generated in the water splitting, which produce the dehydrochlorination of PVC with formation of polyenes.[86]

The process of electrochemical decomposition of the ion-exchange polymer takes place in a very thin near-surface layer of the membrane. That is why the evolution of the surface chemical composition can be detected only by XPS, as in this method the depth of test-beam penetration in the material is only a few nanometers.[89] The application of this method to the fresh and

dx.doi.org/10.1021/jp2101896 |J. Phys. Chem. B 2012, 116, 2145–2161

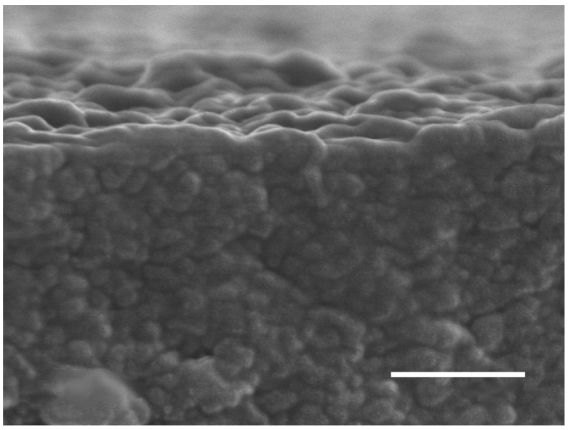

a

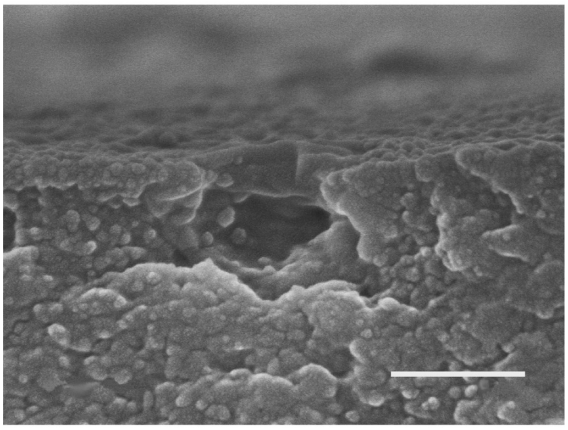

b

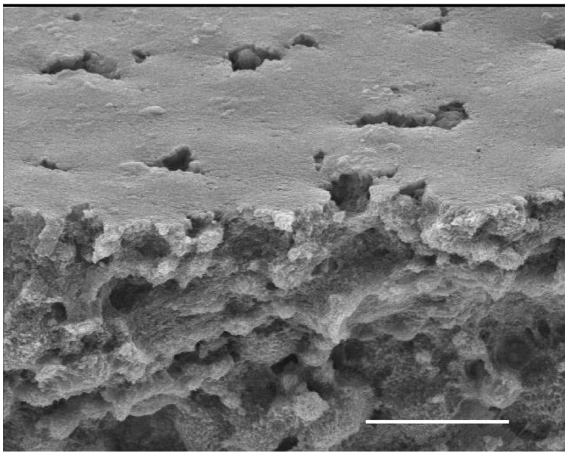

c

Figure 7. SEM images of the CMX membrane cross sections before (a) and after its operation in intensive current regimes during 100 h (b) and 150 h (c). Scale bar = 300 nm (a), 333 nm (b), and 3 μm (c).

treated CMX membranes has shown that after 100 h of operation under current, the concentration of chlorine (which is part of the PVC) has increased by 9% and the concentration of sulfur (which is part of the ion-exchange groups of CMX) has reduced by 15% in a thin surface layer. This result shows that with time of operation, the near-surface layer is enriched in PVC particles and depleted in the ion-exchange groups.

At the same time, FTIR and XFS, which examine the sample for its entire depth (FTIR),[90] or the depth of about 1 μm[90] does not reveal any evolution of the CMX chemical composition and structure during its treatment (as it was also noted by Choi and Moon).[35] Hence, the membrane bulk properties seem to have not changed significantly during the membrane operation under current.

The products of degradation of the ion-conducting polymer might be removed from the membrane surface by the circumambient solution. This would result in increasing the surface fraction of relatively hydrophobic PVC (the water contact angle of the material at 20 °C[91] is equal to 89°). Really, the water contact angle on the membrane surface increases from 32 ± 3° (the fresh membrane) to 49 ± 2° (after 25 h of operation; Table 2). Thus, hydrophobicity of the surface increases during the first 20−25 h of the membrane operation under current.

Apparently, the flow of solution washing the membrane surface removes not only the degraded ion-exchange polymer, but also embedded in it the grains of PVC. This explains the appearance of cavities, observed on the membrane surface (Figures 6b,c, 7b,c, and 8). Hence, a certain dynamic equilibrium is established at the interface. However, the thickness of the membrane should continuously decrease with time. For a Neosepta cation-exchange membrane (having very close to the CMX chemical content of the ion-exchange polymer and PVC particles as filler) we have observed a decrease in the thickness (from 176 to 160 μm) after two years of membrane use in a food desalination industrial process.

It is of interest that the contact angle does not change after 25 h of membrane treatment, while the amount of cavities continues to increase at least up to 150 h. It can be explained by two opposite effects. On the one hand, in the course of time the surface should be enriched with hydrophobic PVC . On the other hand, since the contact angle of the material is less than 90°, the roughness produced by the cavities should increase the hydrophilicity, according to the Wenzel theory.[65,67]

Note that the values of contact angles that we measured on the surface of a swollen in a 0.02 M NaCl solution CMX membrane are 20−30° less than those recorded in the case of an air-dry membrane. For an air-dry unused CMX membrane, we have found the contact angle to be equal to 90 ± 2° in the moment of contact of the droplet with the surface, and 81 ± 2°, 20 s after applying a drop. These results are consistent with those obtained for an AMX membrane by Kang et al.[37] who have found a decrease in the contact angle when passing from a dry to a swollen membrane. We have observed similar behavior in the case of Nafion-117 membrane undergone an oxidation-thermal pretreatment. The observed changes in contact angle with time are due to the increase in the hydrophilic component of surface free energy of the interface due to the hydration of hydrophilic groups in the process of swelling and their reorientation toward the surface.[92,77]

4.2. Evolution with Time of the Current−Voltage Characteristics of CMX Membrane. Figure 9a shows the total and partial (for the H^+ ions) CVC, obtained in a 0.02 M NaCl solution for an unused CMX membrane and the same membrane after 100 h treatment under intensive current $i = 3i_{lim}^{theor}$. The dashed line shows the theoretical limiting current density i_{lim}^{theor} calculated using eq 1. Figure 9b presents the same data in "log(i/i_{lim}^{theor}) − potential difference" coordinates. Roman numerals in Figure 9a indicate the characteristic regions of the CVC: the initial "ohmic" region (I), the plateau or "limiting current" region

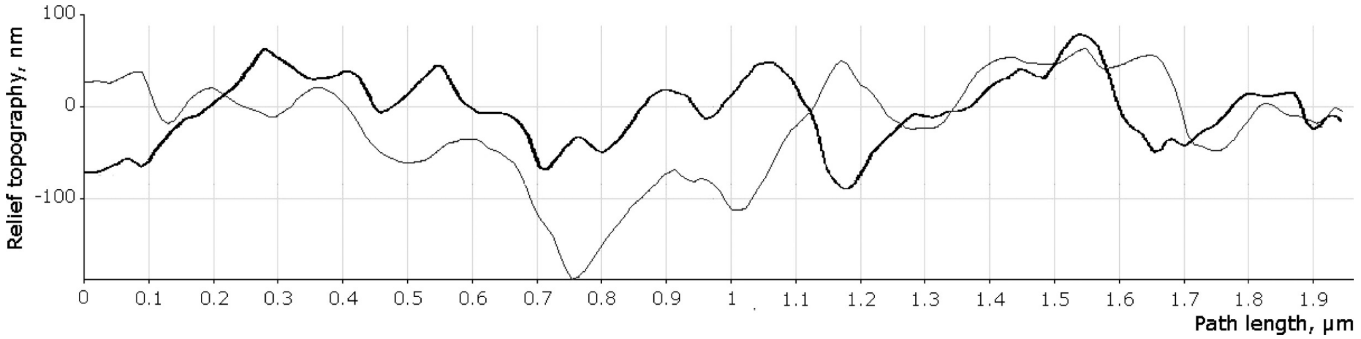

Figure 8. SEM relief of a CMX membrane before (thick line) and after (thin line) its treatment under overlimiting current during 100 h.

Table 2. Contact Angle between Water and the CMX Membrane Surface and Some Other Characteristics of the Membrane as Functions of the Time of Operation under Current

time of the membrane treatment under current, h	contact angle, degrees	surface fraction occupied by cavities, %	plateau length of the CVC (Figure 9), V	$i_{lim}^{exp}/i_{lim}^{theor}$ (Figure 10)
0	32 ± 2	0.013	0.37	1.0
10			1.62	1.1
25	49 ± 2		2.25	1.3
100	49 ± 6	0.4	1.47	1.6
150	49 ± 4	1.8	1.38	2.0

(II), and the "overlimiting" region (III).[11] Open dots denote the experimental limiting current (i_{lim}^{exp}), found by the intersection of the tangents drawn to regions I and II. Filled dots relate to the inflection points corresponding to the transition from region II to region III.

Figure 10 shows the evolution of the CVC of a CMX membrane after 0, 10, 25, 100, and 150 h of its overlimiting current operation. The curves are normalized to i_{lim}^{theor}. The potential difference $\Delta\varphi'$ is reduced in accordance to eq 11.

4.3. Evaluation of Contributions into the Overlimiting Current through the CMX Membrane. The contributions into the overlimiting current may be evaluated with help of eq 8, if the partial current density of water dissociation products (H^+ or OH^- ions), i_w, and the total current density, i, are measured. i_w is found from the mass transfer measurements. Really, the partial current density of counterions i_1 is determined according to eq 13 and the rate of concentration decrease and alkaline (acid) titration in tank (3) (section 3.5). Then $i_w = i - i_1$, and all the terms of eq 8 are found.

The data presented in Figure 9a show that the membrane operation under overlimiting current does not lead to a noticeable change in the rate of H^+ and OH^- ions generation at its interface. This result is consistent with that found by Choi and Moon.[35] Indeed, the partial current of protons before and after the treatment under current is identical within the measurement error; in both cases the water splitting is not intensive, it does not go over 7% (achieved at 3 V of pd across the membrane under study). This means that the main fraction of the current is transferred through the CMX by the sodium ions.

In the case of unused membrane, the value of limiting current density i_{lim}^{exp} determined from the CVC (Figure 9a) and its theoretical value i_{lim}^{theor} are almost identical (Figures 9a, 10). However, even after 10 h of operation under current, i_{lim}^{exp}

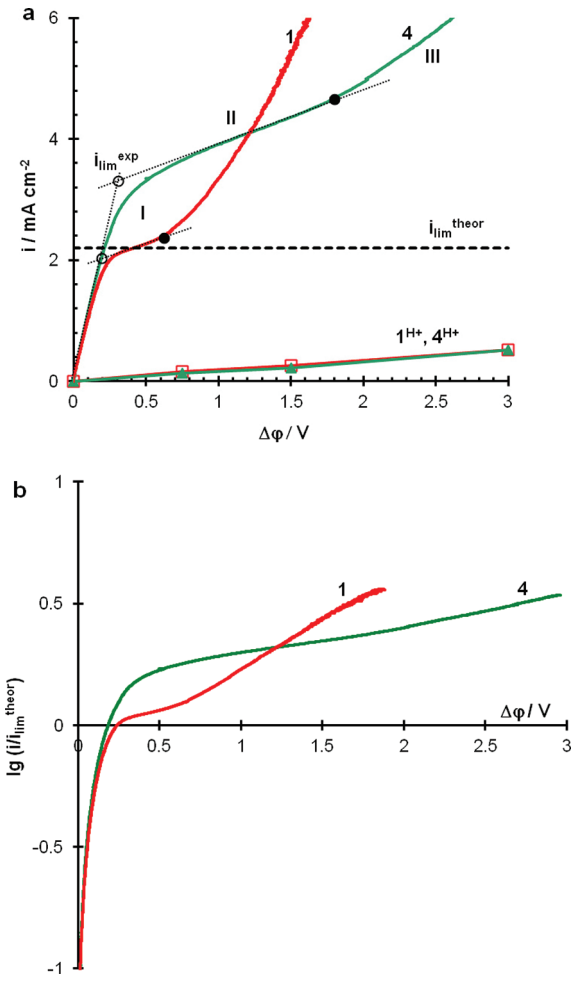

Figure 9. Total (1, 4) and partial (the current density of H^+ ions) (1^{H+}, 4^{H+}) current−voltage characteristics presented as the $I-V$ (a) and the $\log(i/i_{lim}^{theor}) - V$ (b) dependences of an unused (1, 1^{H+}) and a treated at overlimiting current during 100 h (4, 4^{H+}) CMX membrane, in a 0.02 M NaCl solution. The current density of Na^+ counterions, i_{Na+}, is the difference between i_{tot} and i_{H+}. The dashed line shows the theoretical limiting current density, i_{lim}^{theor}, calculated using eq 2. Open dots denote the experimental limiting current, i_{lim}^{exp}. Filled dots relate to the inflection points delimiting regions II and III.

increases by about 5%, and after 25, 100, and 150 h the increase is 30%, 70%, and 100%, compared to i_{lim}^{theor}, respectively.

It is to note that the exaltation current[18] of Na^+ counterions, which is due to the effect of OH^- ions on the electric field in the

dx.doi.org/10.1021/jp2101896 |J. Phys. Chem. B 2012, 116, 2145–2161

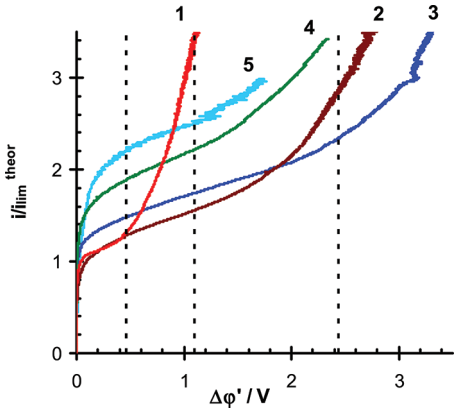

Figure 10. Evolution of the $I-V$ characteristics of the CMX membrane during its overlimiting current operation in a 0.02 M NaCl solution. $\Delta\varphi'$ is the reduced, in accordance with eq 6, potential difference across the membrane under study. Dashed lines denote the values of $\Delta\varphi'$, which were applied when measuring the mass transfer coefficient. Curve 1 relates to the unused membrane, and curves 2−5 relate to 10, 25, 100, and 150 h of membrane treatment at $i = 3i_{lim}^{theor}$, respectively.

depleted DBL, and calculated according to eq 8, does not exceed 1.5% of the total current. Hence, this effect cannot noticeably affect the CVC.

Another effect, which could increase the limiting and overlimiting current, is the flux of salt co-ions through the membrane. This flux is due to back electrolyte diffusion and electromigration transfer of the co-ions through the membrane. The loss in permselectivity, which is due to the co-ion transfer, is added to that caused by water splitting. This overall loss is quantified by the deviation of the salt counterion effective transport number (T_1) from unity. However, the back diffusion is rather low. The diffusion permeability coefficient, P, of the CMX membrane measured (according to the procedure described in section 3.6) under conditions of stationary diffusion from 0.5 M NaCl solution, from one side of the membrane, to pure water, on the other side, is found to be $(3.8 \pm 0.2) \times 10^{-8}$ cm^2 s^{-1} for the "fresh" membrane and $(3.7 \pm 0.2) \times 10^{-8}$ cm^2 s^{-1} for that treated during 100 h under current. We can see that, first, P does not change under the action of overlimiting current (that confirms once more that there are no chemical destruction in the membrane bulk, if the time of membrane operation does not exceed 100 h), and, second, that the current density, which can be transferred by co-ions due to the back diffusion, is too small. This current density calculated as $FP\Delta C/d$, according to eq 3, with $\Delta C = 0.04$ M and $d = 0.0176$ cm, the membrane thickness, is equal to 0.009 mA cm^{-2}. The difference in salt concentration across the membrane is taken two times higher than the bulk concentration because the concentration at the enriched interface at $i = i_{lim}$ doubles the bulk concentration value. This current is very small (<0.45%) compared to the limiting and overlimiting current densities, which exceed 2 mA cm^{-2}. As we have mentioned above, the transport number of counterion in the membrane, $\bar{t}_1$, for membranes similar to CMX is very close to 1. Hence, the effective transport number evaluated by eq 3 should be higher than $(\bar{t}_1 - 0.0045)$. This justifies the value $T_1 = 0.99$ used in evaluation of the limiting current density in section 3.4.

The analysis made above allows us to exclude the decrease in T_{Na+} and the exaltation effect as possible causes for increasing the limiting and overlimiting current density through the CMX membrane. Thus, we can state that, in accordance with eq 8, the main reason for the current density increase over the limiting current is the increase in the salt counterion transfer through the membrane, and this increase is due to reducing effective thickness of the depleted DBL.

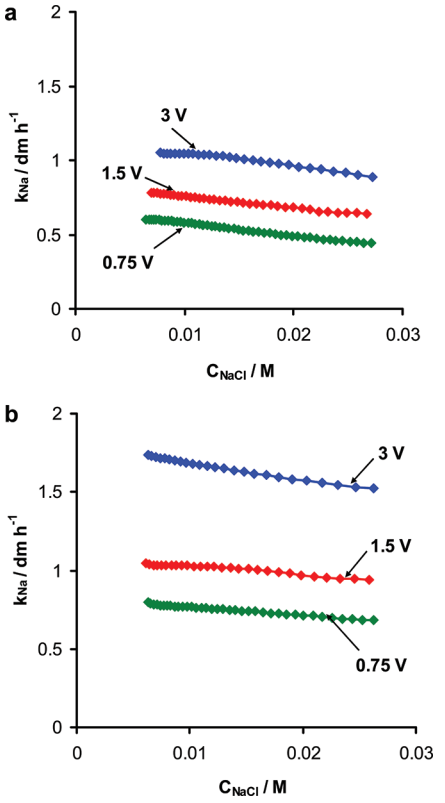

Figure 11. Concentration dependence of Na^+ mass transfer coefficient, measured after 10 h (a) and 100 h (b) of a CMX membrane treatment under overlimiting current. The potential drops applied over the membrane (see Figure 1) were 0.75, 1.5, and 3 V.

4.4. Mass-Transfer Rate. While CVC yields valuable information on the membrane behavior, we can quantify the salt counterion transfer rate through the membrane only after evaluation of other contributions into current transfer: the H^+ and OH^- ions transport due to water splitting, and the co-ion contribution.

The measurement of the rate of solution desalination, as described in section 2.2, gives the direct information on the counterion transfer rate presented here in the form of mass transfer coefficient k_{Na+}. Figure 11 represents the concentration dependence of the Na^+ ion mass transfer coefficient, measured after 10 h (a) and 100 h (b) of the CMX treatment. The data were obtained at the potential difference (registered with Luggin's capillaries as shown in Figure 1) equal to 0.75, 1.5, and 3 V, which correspond to values 0.46, 1.1, and 2.4 V of the reduced potential drop $\Delta\varphi'$ (shown in Figure 11 by dashed lines).

It can be seen that at all applied pd, the mass transfer coefficient is significantly higher for the CMX membrane treated under current during 100 h, in comparison with that treated 10 h. In both cases the value of k_{Na+} exceeds (up to 5 times, Table 3) the theoretical value k_{lim}^{theor}, which can be computed by applying Lévêque's eq 1 for the calculation of limiting current density, and definition $k_1 = (i_1/FC)$, when assuming that no water splitting occurs. In all cases, the gain in mass transfer rate increases with

Table 3. Na^+ Mass Transfer Coefficient across a CMX Membrane, Normalized to the Theoretical Limiting Mass Transfer Coefficient, k_{lim}^{theor}

inlet NaCl concentration, M	time of treatment under current, h	k_{Na^+}/k_{lim}^{theor}		
		0.75 V[a]	1.5 V[a]	3 V[a]
0.02	10	1.3 ± 0.1	1.8 ± 0.1	2.6 ± 0.1
0.02	100	1.9 ± 0.2	2.7 ± 0.2	4.2 ± 0.3
0.005	10	1.6 ± 0.1	2.3 ± 0.2	3.0 ± 0.2
0.005	100	2.3 ± 0.2	3.1 ± 0.2	5.0 ± 0.3

[a] The value of pd between Luggin's capillaries set as shown in Figure 1.

increasing pd and diluting the inlet solution. The first effect is readily explained by the fact that k_{lim}^{theor} is related to the theoretical limiting current, hence, it does not depend of the applied pd as soon as the limiting current is overcome.

The growth of k_{Na+} with diluting solution is explained if one assumes that the main mechanism of the overlimiting mass transfer is electroconvection. Indeed, since the double electric layer thickness increases when the electrolyte concentration decreases (being inversely proportional to $\sqrt{c}$), the thickness of the expended nonequilibrium space charge region at the depleted membrane surface increases with pd more readily with diluting solution.[93,15] The larger the SCR thickness, the more effective is electroosmotic slip because the inhibitory effect produced by the surface due to viscous forces, decreases rapidly with increasing the distance from the surface.

4.5. Mechanism of the Overlimiting Transfer Rate Growth. Since all of the electrochemical experiments (voltammetry, mass transfer measurements, and chronopotentiometry) were conducted under conditions where the gravitational convection was suppressed (the membrane under study was in horizontal position and the lighter depleted diffusion layer was under the membrane), the co-ion transfer is negligible and water splitting has not increased after membrane treatment under current, we can assert that the main reason for enhancement of mass transfer and reducing the effective DBL thickness, δ, eq 4, can only be electroconvection.[93,44,15]

Once this statement is accepted, the question arises: why electroconvection increases with the time of the membrane treatment in overlimiting current mode?

The first explanation is the increase in hydrophobicity of the membrane surface (Table 2). As it was mentioned in section 2, the increase in surface hydrophobicity reduces the forces of attraction between water molecules and the solid surface. Water, driven by the counterions located in the extended SCR near the membrane, slips much easier along a hydrophobic surface. In our paper[15] we have presented several examples showing strong correlation between the degree of surface hydrophobicity (characterized by the contact angle) and the overlimiting transfer rate. There are other studies, which indirectly evidence the effect of membrane surface hydrophobicity on their electrochemical behavior under intensive current regimes. Berezina and collaborators[94,95] have shown that coating the surface of MK-40 and MA-41 ion-exchange membranes with some organic compounds such as camphor entails an increase in the limiting current density found from CVC, as well as activation of microconvective flows near the surface detected by laser interferometry. Apparently, these effects may be explained by the fact that camphor molecules are hydrophobic that facilitates electroconvective slip of solution near the surface.

Balster et al.[13] note that the plateau length in the CVC of an experimental S-PEEK membrane depends on whether the membrane surface exposed to the current was addressed to air atmosphere or to glass during the polymerization. The plateau length is longer for freshly prepared membranes, if the exposed to the current surface was addressed to glass. Moreover, the plateau becomes longer with increasing degree of sulfonation and with increasing time of keeping the membrane in water solutions. The authors[13] explain the observed effects by different surface heterogeneity of the membranes prepared in different conditions. However, the role of hydrophobicity may also be important in the considered cases. Really, additional sulfonation and the contact with water increase the surface hydrophilicity; the latter is due to reorientation of the polymer chains and the tendency of fixed ions to reach water solution. Higher hydrophilicity of the surface results in higher voltage needed for arising electroconvection, consequently, this leads to stretching out the plateau length.

However, the explanation of the growth of overlimiting transfer through the treated CMX membrane, which is based only on the role of surface hydrophobicity, is not sufficient because the contact angle increases only during few tens of hours (Table 2), whereas the growth of overlimiting transfer rate continues at least during 150 h of the operation. Apparently, it is the effect of surface morphology variation, which is also important.[11,13]

The effect of surface roughness on the flow generation by an electric field is an important factor for developing microfluidic devices.[96] However, the situation is not sufficiently clear, and opposing experimental results have been obtained. Bonaccurso et al.[97] reported that roughness generates extremely large slip, whereas Granick et al.[98] wrote that it decreases the degree of slippage. From the theoretical point of view, to better understand the phenomenon, it is necessary to apply models with a slip condition on the wall like that presented by eq 10.[99,96]

The cavities, which make the surface undulated, might be responsible for the overlimiting transfer growth after reaching certain constant degree of surface hydrophobicity. Indeed, as the SEM visualization of the surface shows, the number of cavities per unit surface and their size increase with the time of membrane treatment under current. As for the role of the cavities in the mass transfer enhancement, a possible mechanism is shown in Figure 12. As we have mentioned in section 2.3, if the geometry of conducting surface is so that a tangential electric field is applied upon an extended SCR at a sloping surface, the electroconvective transfer is much stronger than near a flat surface.[44,11,100,48,13]

Paired vortices within a cavity enhance the delivery of "fresh" solution from the bulk. Due to viscous friction, these vortices may give rise to other pairs of vortices at the flat part of the surface as shown in Figure 12. The rising of the vortices at the "elevated plane" is easier when the surface is more hydrophobic. Apparently, the vortices rotating within the cavity not only enhance the mass transfer but facilitate also the removal of the products of polymer destruction from the cavity and contributes to increasing the cavity's width and depth.

Another important point is concerned with earlier onset of electroconvection. As the bottom of a cavity is at certain distance from the elevated plane, the electrolyte concentration and, hence, the local limiting current density here is lower than at the plane. As a consequence, the conditions sufficient for the onset of electroconvection of the second kind are attained in the cavity at a lower voltage in comparison with the elevated plane having flat

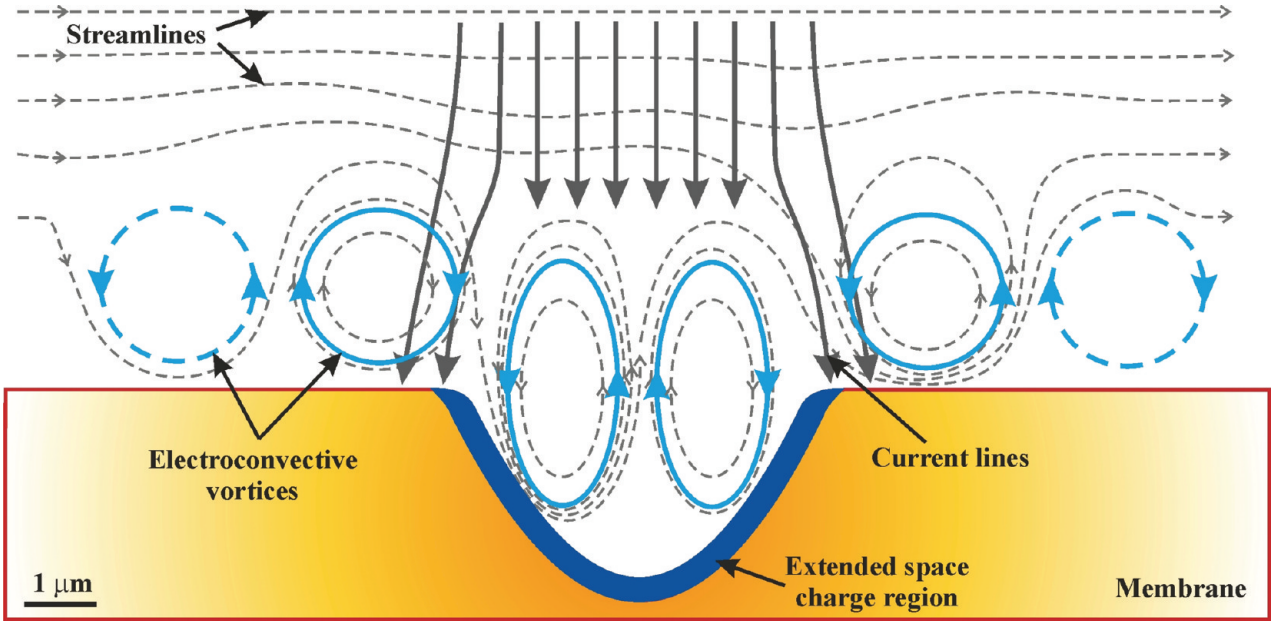

Figure 12. Possible mechanism of occurring paired electroconvective vortices on the surface of ion-exchange membrane under an electric current directed normally to the membrane surface. Streamlines and electric current lines are shown schematically.

surface. In other words, electroconvection in a cavity arises at lower voltage than that corresponding to the beginning of regime II[11] near the flat elevated surface. The cavity-inside vortices enhance the electrolyte delivery to the flat regions of the surface that is equivalent to a decrease in δ and an increase in i_{lim} when the system globally remains in regime I (Figure 9). In this way, it is possible to explain the growth in limiting current density corresponding to the passage from regime I to regime II according to the theory by Rubinstein and Zaltzman.[11] As well the passage from regime II to regime III appears to be shifted to higher currents.

The mechanism of increasing overlimiting transfer presented above finds some support in the variation of the shape of ChP curves with the time of CMX operation under current (Figure 13). In the case of a little-used membrane ($CMX_{t=5hrs}$), the transition state where the electrolyte concentration approaches zero at a rather high current density ($i = 3\ i_{lim}^{theor}$) is attained nearly simultaneously over all the surface. The pd increases rapidly with time, and the transition time is close to that calculated according to the Sand equation deduced for a semi-infinite 1D diffusion

$$\tau = \left(\frac{\pi D}{4}\right)\left(\frac{C_i^0 z_i F}{T_i - t_i}\right)^2 \frac{1}{i^2} \qquad (15)$$

If the membrane was operated under current and a number of cavities formed on the surface ($CMX_{t=150\ h}$), the beginning of the curve is close to that of $CMX_{t=5\ h}$. However, the transition state of $CMX_{t=150\ h}$ is found to be stretched in time. This is apparently due to the formation of vortices enhancing electrolyte delivery to the surface and reducing pd. The formation of vortices needs time; their rotation slows down the growth of concentration polarization. As a result, the time for attaining a stationary state in the system is significantly higher. The situation is similar to that occurring in the case of heterogeneous MK-40 membrane, investigated earlier[58] (Figure 13). The surface of this membrane

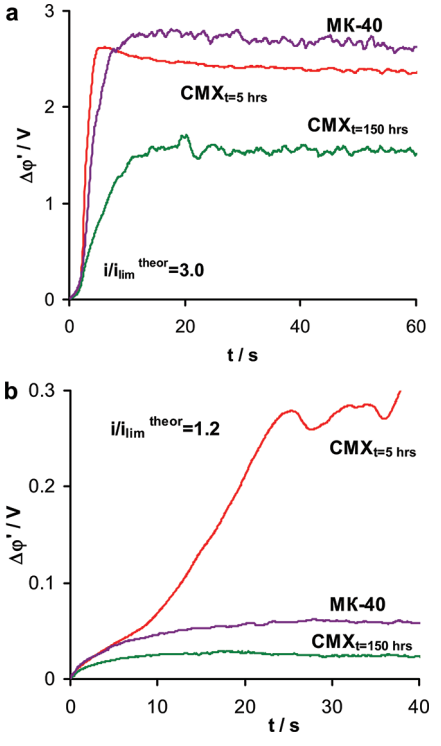

Figure 13. Chronopotentiograms of a homogeneous CMX and a heterogeneous MK-40 membranes, obtained at current densities equal (a) to 6.7 mA/cm^2 (3 i_{lim}^{theor}) and (b) to 2.6 mA/cm^2 (1.2 i_{lim}^{theor}). Before the experiment the samples of CMX membrane were treated under current $i = 3i_{lim}^{theor}$ during 5 h ($CMX_{t=5\ h}$) or 150 h ($CMX_{t=150\ h}$). $\Delta\varphi'$ is the reduced pd according to eq 12.

is mainly covered with nonconducting polyethylene (which is used as a strengthening filler), and about 25% of the surface is occupied with conducting cation-exchange particles of 20−30 μm in diameter.[12,58] It can be expected that these particles play

the role similar to that of the cavities on the CMX surface: just near these particles electroconvective vortices arise since the current lines condense here (funneling effect[57,101,58]) causing formation of expanded SCR. There is however a difference: as the surface covered by polyethylene is not conducting, the local current density through the ion-exchange particles is several times higher than that through the CMX cavities, under the same average current density. This results in higher concentration polarization, hence, higher pd. Besides, the presence of polyethylene gives rise to tangential diffusion, which increases the transition time and makes the ChP curve more diffuse.[101,58] The occurrence of nonstationary electroconvection at CMX $_{t=150\ h}$ and MK-40 membranes is evidenced by the pd oscillations quite similar in both cases. However, the higher concentration polarization of the MK-40 membrane caused by too small fraction of its conducting surface results in higher pd exceeding also that of $CMX_{t=5\ h}$.

It is also of interest to compare the ChP curves of $CMX_{t=5\ h}$ and $CMX_{t=150\ h}$ at a current density slightly (by 20%) surpassing i_{lim}^{theor} (Figure 13b). In this case, the ChP curves of CMX_S has an inflection point indicating the passage through limiting current density. The ChP curves of $CMX_{t=150\ h}$ has not this point. Hence, the electroconvective vortices under this current density arise at so low pd that the limiting current regime on the elevated plane remains rather far. However, small oscillations in the ChP curve of $CMX_{t=150\ h}$ at times higher than 10 s (which is lower than the transition time for an ideal flat surface, according to the Sand equation) indicate the presence of electroconvection.

5. CONCLUSIONS

We have found that the overlimiting mass-transfer rate through a CMX membrane increases after its operation in overlimiting current mode in a dilute (equal or less than 0.02 M) NaCl solutions. The main mechanism of overlimiting transfer in the conditions of experiments is electroconvection. The increase of overlimiting mass-transfer is apparently caused by growing surface hydrophobicity and by appearing cavities of micrometer scale. The both variations in surface properties are due to degradation, under the action of intensive current density, of cation-exchange polymer (sulfonated styrene-divinylbenzene) making a continuous phase of the CMX. The erosion of this hydrophilic phase causes increasing presence on the surface of another membrane component, which is relatively hydrophobic PVC in the form of small (about 100 nm) particles. More hydrophobic surface facilitates the electroosmotic slip of water. Washing-out of PVC particles gives rise to formation of cavities. Tangential electric force applied to the extended space charge region at sloping walls of a cavity generates paired electroconvective vortices, which bring in motion the liquid inside the cavity and near the flat elevated surface around the cavity. On the other hand, these vortices accelerate the surface erosion increasing the number and the size of cavities.

Since the space inside a cavity is less available for the "fresh" solution, the concentration polarization of its bottom and walls is higher than that of the elevated flat surface. As a consequence, an extended SCR and, hence, electroconvection arise in a cavity when the current density on the elevated flat surface is lower than i_{lim}. This explain the increase of globally underlimiting regime I (if using the terminology according to the theory of Rubinstein and Zaltzman[11]), and the rise of the limiting current density separating regimes I and II in the $I-V$ curve. Moreover, all three characteristic regimes in the $I-V$ curve are observed shifted to higher currents. We have found that i_{lim} through the CMX has increased in about 2 times after 150 h of overlimiting current operation, while i_{lim} is quite close to i_{lim}^{theor} (calculated according to the Lévêque equation) for an unused CMX membrane. At higher voltages (3 V over a membrane, which corresponds to regime III in the $I-V$ curve) the Na^+ mass transfer coefficient through the CMX after 150 h of current operation was found 5 times higher than the theoretical limiting value calculated with the use of the Lévêque equation.

AUTHOR INFORMATION

Corresponding Author

*E-mail: v_nikonenko@mail.ru. Phone/Fax: +7 861 219 95 73.

ACKNOWLEDGMENT

Part of the work was carried out within the framework of joint Russian−French laboratory "Ion-Exchange Membranes and Related Processes". The authors are grateful to the CNRS, RFBR (Grant Nos. 11-08-93107-NCNIL-a, 11-08-96511, and 11-08-00599-a), and FP7 Marie Curie Actions "CoTraPhen" Project PIRSES-GA-2010-269135.

ABBREVIATIONS

CA: contact angle
ChP: chronopotentiometric curve
CVC: current−voltage curve
DBL: diffusion boundary layer
DC: desalination channel
ED: electrodialysis
EDL: electric double layer
FTIR: Fourier transform infrared spectroscopy
IEM: ion-exchange membrane
pd: potential difference
PVC: polyvinylchloride
SCR: space charge region
SEM: scanning electron microscopy
XFS: X-ray fluorescence spectroscopy
XPS: X-ray photoelectron spectroscopy

Symbols

b: slip length
C: electrolyte concentration
ΔC: concentration difference
D: electrolyte diffusion coefficient
F: Faraday constant
f_c: surface fraction of conducting area
g: free-fall acceleration
Gr: Grashof number
h: spacing between the membranes
i: electric current density
i_{av}: average current density
J_i: flux density of ion i
k_1: mass transfer coefficient
L: length of desalination channel
Ra: Rayleigh number
Ra_{cr}: critical Rayleigh number
R_{ef}: differential resistance of the membrane system
S: polarized membrane surface area
Sc: Schmidt number

t: time
T_1 effective transport number of the counterion in the membrane
t_1: transport number of the counterion in solution
$\overline{t}_1$: transport number in the membrane
u_{slip}: fluid tangential velocity at the surface
V: flow velocity
V_{sol}: volume of solution in the desalting stream
X_0: characteristic distance

Greek Symbols

δ: thickness of the Nernst diffusion boundary layer
ν: kinematic viscosity
ρ: solution density
$\Delta\varphi'$: reduced value of potential drop
$\Delta\varphi_{ohm}$: ohmic resistance of the nonpolarized membrane system
$\Delta\varphi_{tot}$: total potential drop

Indexes: Subscripts

0: related to the solution bulk
1: salt counterion
i: ion number
Lev: value, calculated according to Lévêque equation
lim: related to the limiting current
loc: local value
s: related to the surface
w: related to water splitting

Indexes: Superscripts

A: anion-exchange membrane
C: cation-exchange membrane
exp: experimental data
theor: theoretical data

REFERENCES

(1) Electrodialysis and electrodialysis reversal (M38); AWWA manual 2007; p 62.
(2) Valero, F.; Arbós, R. *Desalination* **2010**, *253* (1−3), 170–174.
(3) Vera, E.; Sandeaux, J.; Persin, F.; Pourcelly, G.; Dornier, M.; Piombo, G.; Ruales, J. *J. Food Eng.* **2007**, *78*, 1427–1438.
(4) Soares, P. A. M. H.; Geraldes, V.; Fernandes, C.; Cameira dos Santos, P.; Norberta de Pinho, M. *Am. J. Enol. Vitic.* **2009**, *60*, 183–188.
(5) Nagarale, R. K.; Gohil, G. S.; Shahi, V. K. *Adv. Colloid Interface Sci.* **2006**, *119*, 97–130.
(6) Strathmann, H. Electromembrane Processes: Basic Aspects and Applications. In *Comprehensive Membrane Science and Engineering*; Drioli, E., Giorno, L., Eds.; Elsevier Science: Amsterdam, 2010; Vol. 2, pp 391−429.
(7) Wang, Y.; Huang, Ch.; Xu, T. *J. Membr. Sci.* **2011**, *374*, 150–156.
(8) Macedonio, F.; Drioli, E. *Membr. Water Treatment* **2010**, *1*, 75–81.
(9) Wood, J.; Gifford, J.; Arba, J.; Shaw, M. *Desalination* **2010**, *250*, 973–976.
(10) Anderson, M. A.; Cudero, A. L.; Palma, J. *Electrochim. Acta* **2010**, *55*, 3845–3856.
(11) Rubinstein, I.; Zaltzman, B. *Phys. Rev. E.* **2000**, *62*, 2238–2251.
(12) Belova, E.; Lopatkova, G.; Pismenskaya, N.; Nikonenko, V.; Larchet, C.; Pourcelly, G. *J. Phys. Chem. B* **2006**, *110*, 13458–13469.
(13) Balster, J.; Yildirim, M. H.; Stamatialis, D. F.; Ibanez, R.; Lammertink, R. G. H.; Jordan, V.; Wessling, M. *J. Phys. Chem. B* **2007**, *111*, 2152–2165.
(14) Urtenov, M. A.-K.; Kirillova, E. V.; Seidova, N. M.; Nikonenko, V. V. *J. Phys. Chem. B* **2007**, *111*, 14208–14222.
(15) Nikonenko, V. V.; Pismenskaya, N. D.; Belova, E. I.; Sistat, Ph.; Huguet, P.; Pourcelly, G.; Larchet, Ch. *Adv. Colloid Interface Sci.* **2010**, *160*, 101–123.
(16) Simons, R. *Electrochim. Acta* **1984**, *29*, 151–158.
(17) Sheldeshov, N. V.; Ganych, V. V.; Zabolotskii, V. I.; Russ., J. *Electrochem.* **1991**, *27*, 11–15.
(18) Kharkats, Yu. I.; Russ., J. *Electrochemistry* **1985**, *21*, 917–920.
(19) Guyon, E., Hulin, J.-P., Petit, L., Eds.; *Hydrodynamique physique. Matiere Condensee. Savoirs Actuels InterEditions*; CNRS: Paris, 2001; p 563.
(20) Volgin, V. M.; Davydov, A. D.; Russ., J. *Electrochemistry* **2006**, *42*, 567–608.
(21) Zabolotsky, V. I.; Nikonenko, V. V.; Pismenskaya, N. D. *J. Membr. Sci.* **1996**, *119*, 171–181.
(22) Zabolotsky, V. I.; Nikonenko, V. V.; Pismenskaya, N. D.; Laktionov, E. V.; Urtenov, M. Kh.; Strathmann, H.; Wessling, M.; Koops, G. H. *Sep. Purif. Technol.* **1998**, *14*, 255–267.
(23) Strathmann, H. *Desalination* **2010**, *264*, 268–288.
(24) Tanaka, Y. *J. Membr. Sci.* **2010**, *350*, 347–360.
(25) Rubinstein, S. M.; Manukyan, G.; Staicu, A.; Rubinstein, I.; Zaltzman, B.; Lammertink, R. G. H.; Mugele, F.; Wessling, M. *Phys. Rev. Lett.* **2008**, *101*, 236101−1−4.
(26) Yossifon, G.; Mushenheim, P.; Chang, Y.-C.; Chang, H.-C. *Phys. Rev. E* **2010**, *81*, 046301−1−13.
(27) Nikonenko, V. V.; Pismenskaya, N. D.; Istoshin, A. G.; Zabolotsky, V. I.; Shudrenko, A. A. *Chem. Eng. Process: Process Intensification* **2008**, *47*, 1118–1127.
(28) Bazant, M. Z.; Kilic, M. S.; Storey, B. D.; Ajdari, A. *Adv. Colloid Interface Sci.* **2009**, *152*, 48–88.
(29) Kim, D.; Posner, J. D.; Santiago, J. G. *Sens. Actuators A* **2008**, *141*, 201–212.
(30) Mishchuk, N. A.; Heldal, T.; Volden, T.; Auerswald, J.; Knapp, H. *Microfluid Nanofluid* **2011**, *11*, 1–10.
(31) Tallarek, U.; Leinweber, F. C.; Nischang, I. *Electrophoresis* **2005**, *26*, 391–404.
(32) Mishchuk, N. A.; Heldal, T.; Volden, T.; Auerswald, J.; Knapp, H. *Electrophoresis* **2009**, *30*, 3499–3506.
(33) Kim, S.-J.; Ko, S.-H.; Kang, K.-H.; Han, J. *Nat. Nanotechnol.* **2010**, *5*, 297–301.
(34) Dammak, L.; Larchet, Ch.; Grande, D. *Sep. Purif. Technol.* **2009**, *69*, 43–47.
(35) Choi, J.-H.; Moon, S.-H. *J. Colloid Interface Sci.* **2003**, *265*, 93–100.
(36) Franck-Lacaze, L.; Bonnet, C.; Choi, E.; Moss, J.; Pontvianne, S.; Poirot, H.; Datta, R.; Lapicque, F. *Int. J. Hydrogen Energy* **2010**, *35*, 10472–10481.
(37) Kang, M.-S.; Choi, Y.-J.; Moon, S.-H. *AIChE J.* **2003**, *49*, 3213–3220.
(38) Levich, V. G. *Physicochemical hydrodynamics*; Prentice Hall: Englewood Cliffs, NJ, 1962; p 700.
(39) Newman, J. S. *Electrochemical systems*; Prentice Hall: Englewood Cliffs, NJ, 1973; p 309.
(40) Helfferich, F. G. *Ion Exchange*; McGraw-Hill: New York, 1962; p 624.
(41) Larchet, C.; Dammak, L.; Auclair, B.; Parchikov, S.; Nikonenko, V. *New J. Chem.* **2004**, *28*, 1260–1267.
(42) Gnusin, N. P.; Zabolotskii, V. I.; Nikonenko, V. V.; Urtenov, M. Kh. *Sov. Electrochem.* **1986**, *23*, 273–278.
(43) Peers, A. M. *Discuss. Faraday Soc.* **1956**, *21*, 124–125.
(44) Mishchuk, N. A. *Adv. Colloid Interface Sci.* **2010**, *160*, 16–39.
(45) Rubinstein, I.; Shtilman, L. *J. Chem. Soc. Faraday Trans.* **1979**, *75*, 231–246.
(46) Rubinstein, I.; Zaltzman, B.; Kedem, O. *J. Membr. Sci.* **1997**, *125*, 17–21.
(47) Pismenskaya, N. D.; Nikonenko, V. V.; Belova, E. I.; Lopatkova, G. Yu.; Sistat, P; Pourcelly, G; Larshe, K.; Russ., J. *Electrochem.* **2007**, *43*, 307–327.
(48) Dukhin, S. S. *Adv. Colloid Interface Sci.* **1991**, *35*, 173–196.
(49) Mishchuk, N. A.; Dukhin, S. S. *Electrokinetic phenomena of the second kind. In Interfacial Electrokinetics and Electrophoresis*; Delgado, A., Ed.; Marcel Dekker: New York, 2002; pp 241−275.

(50) Squires, T. M.; Bazant, M. Z. J. *Fluid Mech.* **2004**, *509*, 217–252.
(51) Leinweber, F. C.; Tallarek, U. *J. Phys. Chem. B* **2005**, *109*, 21481–21485.
(52) Rubinstein, I.; Zaltzman, B. *Surface chemistry and electrochemistry of membranes*; Sorensen, S., Ed.; Marcel Dekker: New York, 1999; pp 591−621.
(53) Rubinstein, I.; Zaltzman, B.; Lerman, I. *Phys. Rev. E* **2005**, *011505*, 1–19.
(54) Zabolotsky, V. I.; Nikonenko, V. V.; Pismenskaya, N. D.; Pismensky, V. F.; Lactionov, E. V. Patent 2033850 C1 Russian Federation, MPK6 B01D61/46. Electrodialyser. IP Membrane Technology. Krasnodar, Russia, No. 93006226/26; priority 04.02.1993; publication 30.04.1995.
(55) Larchet, C.; Zabolotsky, V. I.; Pismenskaya, N.; Nikonenko, V. V.; Tskhay, A.; Tastanov, K.; Pourcelly, G. *Desalination* **2008**, *222*, 489–496.
(56) Eigenberger, G.; Strathmann, H.; Grabovskiy, A. Patent WO 2005/009596 A1 Germany, B01D 61/44. Membrane assembly, electrodialysis device and method for continuous electrodialytic desalination. Stuttgart University, Germany, No. PCT/EP2004/007961; priority 18.07.2003; publication 03.02. 2005.
(57) Rubinstein, I.; Zaltzman, B.; Pundik, T. *Phys. Rev. E* **2002**, *65*, 041507–1−7.
(58) Volodina, E.; Pismenskaya, N.; Nikonenko, V.; Larchet, C.; Pourcelly, G. *J. Colloid Interface Sci.* **2005**, *285*, 247–258.
(59) Bazant, M. Z.; Vinogradova, O. I. *J. Fluid Mech.* **2008**, *613*, 125–134.
(60) Thompson, P.; Troian, S. *Nature* **1997**, *389*, 360–362.
(61) Churaev, N.; Sobolev, V.; Somov, A. *J. Colloid Interface Sci.* **1984**, *97*, 574–581.
(62) Choi, C.-H.; Westin, K. J. A.; Breuer, K. S. *Phys. Fluids* **2003**, *15*, 2897–2902.
(63) Majumder, M.; Chopra, N.; Andrews, R.; Hinds, B. J. *Nature* **2005**, *438*, 44–44.
(64) Vinogradova, O. I.; Yakubov, G. E. *Langmuir* **2003**, *19*, 1227–1234.
(65) Quere, D. *Physica A* **2002**, *313*, 32–46.
(66) Voronov, R. S.; Papavassiliou, D. V.; Lee, L. L. *Ind. Eng. Chem. Res.* **2008**, *47*, 2455–2477.
(67) Wenzel, R. N. *Ind. Eng. Chem.* **1936**, *28*, 988–994.
(68) Vinogradova, O. I.; Bunkin, N. F.; Churaev, N. V.; Kiseleva, O. A.; Lobeyev, A. V.; Ninham, B. W. *J. Colloid Interface Sci.* **1995**, *173*, 443–447.
(69) Choi, J.-H.; Lee, H.-J.; Moon, S.-H. *J. Colloid Interface Sci.* **2001**, *238*, 188–195.
(70) ASTOM Corporation. Ion exchange membranes production of NEOSEPTA. URL: http://www.astom-corp.jp/en/en-main2-neosepta.html.
(71) Lue, S. J.; Wang, F. J.; Hsiaw, S.-Y. *J. Membr. Sci.* **2004**, *240*, 149–158.
(72) Krol, J. J.; Wessling, M.; Strathmann, H. *J. Membr. Sci.* **1999**, *162*, 155–164.
(73) Dlugolecki, P.; Anet, B.; Metz, S. J.; Nijmeijer, K.; Wessling, M. *J. Membr. Sci.* **2010**, *346*, 163–171.
(74) Zabolotsky, V. I.; Sheldeshov, N. V.; Gnusin, N. P. *Russ. Chem. Rev.* **1988**, *57*, 801–808.
(75) Nebavsky, A. V.; Shevtsova, K. A.; Pismenskaya, N. D.; Nikonenko, V. V. Ion transport in organic and inorganic membranes: conference proceedings; Bocanova: Krasnodar, 2010; p 121.
(76) Bass, M.; Berman, A.; Singh, A.; Konovalov, O.; Freger, V. *J. Phys. Chem. B* **2010**, *114*, 3784–3790.
(77) Goswami, Sh.; Klaus, Sh.; Benziger, J. *Langmuir* **2008**, *24*, 8627–8633.
(78) Moilanen, D. E.; Piletic, I. R.; Fayer, M. D. *J. Phys. Chem. A.* **2006**, *110*, 9084–9088.
(79) Gebel, G.; Lyonnard, S.; Mendil-Jakani, H.; Morin, A. *J. Phys.: Condens. Matter* **2011**, *23*, 234107–7.
(80) Pismenskaya, N. D.; Nikonenko, V. V.; Melnik, N. A.; Belova, E. I. Patent 100276 Russian Federation, MPK G01N27/40 (2006.01). Device for the integrated study of mass transfer and electrochemical characteristics of ion-exchange membrane. Kuban state university, Krasnodar, Russia, No. 2010129861/28; priority 16.07. 2010; publication 10.12. 2010.
(81) Larchet, C.; Nouri, S.; Auclair, B.; Dammak, L.; Nikonenko, V. *Adv. Colloid Interface Sci.* **2008**, *139*, 45–61.
(82) Robinson, R. A.; Stokes, R. H. *Electrolyte Solutions*; Butterworths: London, 1968; p 571.
(83) Lactionov, E. V.; Pismenskaya, N. D.; Nikonenko, V. V.; Zabolotsky, V. I. *Desalination* **2002**, *152*, 101–116.
(84) Nikonenko, V. V.; Pismenskaya, N. D.; Vedernikova, E. E. Patent 100275 Russian Federation, MPK G01N27/40 (2006.01). Device for measuring the diffusion characteristics of membranes. Kuban state university, Krasnodar, Russia, No. 2010121195/28; priority 25.05.2010; publication 10.12. 2010.
(85) Berezina, N. P.; Timofeev, S. V.; Kononenko, N. A. *J. Membr. Sci.* **2002**, *209*, 509–518.
(86) Sata, T.; Tsujimoto, M.; Yamaguchi, T.; Matsusaki, K. *J. Membr. Sci.* **1996**, *112*, 161–170.
(87) Mizutani, Y. *J. Membr. Sci.* **1990**, *49*, 121–144.
(88) Collier, A.; Wang, H.; Zi Yuan, X.; Zhang, J.; Wilkinson, D. P. *Int. J. Hydrogen Energy* **2006**, *31*, 1838–1854.
(89) *Surface Analysis by Auger and X-ray Photoelectron Spectroscopy*; Grant, J. T., Briggs, D., Eds.; IM Publications and Surface Spectra: Chichester U.K., 2003; p 619.
(90) Harvey, D. *Modern analytical chemistry*; McGraw-Hill: Boston, 2000; p 816.
(91) Boulange-Petermann, L.; Debacq, C.; Poiret, P.; Cromières, B. In *Contact angle, wettability and adhesion*; Mittal, K. L., Ed.; VSP/Brill: Leiden, 2003; Vol. 3, pp 501−519.
(92) Zawodzinski, T. A., Jr.; Springer, T. E.; Davey, J.; Jestel, R.; Lopez, C.; Valerio, J.; Cottesfield, S. *J. Electrochem. Soc.* **1993**, *140*, 1981–1985.
(93) Rubinshtein, I.; Zaltzman, B.; Pretz, J.; Linder, C. *Russ. J. Electrochem.* **2002**, *38*, 853–863.
(94) Berezina, N. P.; Kononenko, N. A.; Dyomina, O. A.; Gnusin, N. P. *Adv. Colloid Interface Sci.* **2008**, *139*, 3–28.
(95) Kononenko, N. A.; Berezina, N. P.; Loza, N. V. *Colloids Surf.* **2004**, *239*, 59–64.
(96) Vinogradova, O. I.; Belyaev, A. V. *J. Phys.: Condens. Matter* **2011**, *23*, 184104–15.
(97) Bonaccurso, E.; Butt, H. J.; Craig, V. S. *J. Phys. Rev. Lett.* **2003**, *90*, 144501–4.
(98) Granick, S.; Zhu, Y.; Lee, H. *Nat. Mater.* **2003**, *2*, 221–227.
(99) Feuillebois, F.; Bazant, M. Z.; Vinogradova, O. I. *Phys. Rev. E* **2010**, *82*, 055301–4.
(100) Zaltzman, B.; Rubinstein, I. *J. Fluid Mech.* **2007**, *579*, 173–226.
(101) Pismenskaia, N.; Sistat, P.; Huguet, P.; Nikonenko, V.; Pourcelly, G. *J. Membr. Sci.* **2004**, *228*, 65–76.